J. Fluid Mech. (1992), *vol.* 244, *pp.* 649–676

Properties of strongly nonlinear vortex/Tollmien–Schlichting-wave interactions

By A. G. WALTON[1] AND F. T. SMITH[2]

[1]Department of Mathematics, Imperial College, London SW7 2BZ, UK

[2]Department of Mathematics, University College London, Gower Street, London WC1E 6BT, UK

(Received 23 October 1991 and in revised form 1 May 1992)

An analytical and computational study is presented on solution properties of strongly nonlinear vortex/wave interactions involving Tollmien–Schlichting waves, in boundary-layer transition. The longitudinal vortex part, i.e. the total mean flow, is governed by a three-dimensional vortex system but coupled, through an effective spanwise slip condition at the surface, with the accompanying wave part, so that both the vortex and the wave parts are unknowns. Terminal forms of the space-marching or time-marching problem are proposed first, yielding either a lift-off separation singularity or a strong-attachment singularity. Second, a similarity version of the complete system is addressed numerically and analytically. This leads to a number of interesting solution features as the typical wave pressure is increased into the strongly nonlinear regime. In particular, lift-off separation and attachment forms seem to emerge which are analogous with those proposed above. The flow developments beyond the terminal forms are discussed, together with the links of the work with recent computational results and, tentatively, with experimental observations including the creation of lambda vortices (as a form of lift-off separation).

1. Introduction

The present paper concerning laminar–turbulent transition describes a study of solution properties, and their interpretations, for strongly nonlinear vortex/wave interactions in cases where the nonlinear wave contribution is of the Tollmien–Schlichting (TS) type. The term 'strongly nonlinear' refers to effects of relative order unity on the total mean flow, locally or globally, so that the mean flow cannot be represented as a small perturbation of the original steady flow, say. This theoretical work follows on from the approximately simultaneous investigations by Smith & Walton (1989), Bennett, Hall & Smith (1991), Hall & Smith (1991) who consider strongly nonlinear interactions following on, in turn, from the weakly nonlinear vortex/wave-interaction studies of Hall & Smith (1988, 1989, 1990), Smith & Blennerhassett (1992). In particular Smith & Walton (1989) describe a range of nonlinear vortex/wave interactions for various input amplitudes and spectra of three-dimensional disturbances to a boundary layer, culminating with the most powerful interaction which is the case of interest here: see below. Boundary-layer flows, and to a lesser extent channel and pipe flows, form the main focus, while Walton (1991) discusses special applications to entry flow in pipes.

Vortex/wave interactions incorporating strong nonlinearity are of much interest from the theoretical and the experimental standpoints because they show how rather

tiny three-dimensional disturbances can affect the mean flow substantially as opposed to weakly. Indeed, such interactions and consequent mean-flow effects seem to have been observed experimentally e.g. in Swearingen & Blackwelder (1987), Aihara, Tomita & Ito (1985), Holden (1985). The potential power of longitudinal vortex/wave interactions is perhaps most easily seen in vortex/Rayleigh-wave cases, which are presented by Hall & Smith (1991) for incompressible or compressible boundary layers. Thus a longitudinal vortex system (the mean flow) filling the entire boundary layer typically has spanwise velocities of order $Re^{-\frac{1}{2}}$ times the free-stream speed ($u_{\rm ref}$), where Re is the large global Reynolds number. The spanwise momentum force is therefore of order $Re^{-\frac{1}{2}}u_{\rm ref}^2/l_{\rm ref}$ for a streamwise lengthscale $l_{\rm ref}$. If in addition a three-dimensional Rayleigh-wave disturbance is present its lengthscales are all of order $Re^{-\frac{1}{2}}l_{\rm ref}$ and so, if the disturbance velocity scale is a fraction κ of $u_{\rm ref}$, the contribution to the main spanwise momentum force produced inertially is $\kappa^2 u_{\rm ref}^2/(Re^{-\frac{1}{2}}l_{\rm ref})$. This suggests that the fraction κ need be only $O(Re^{-\frac{1}{2}})$ for there to be a strongly nonlinear interaction. A detailed examination (Hall & Smith 1991; Brown, Brown & Smith 1992) accounting for the irregular solution response at the critical layer then modifies the above finding slightly, showing that in fact κ is $O(Re^{-\frac{7}{12}})$. The main point, however, is that κ need only be relatively tiny in practical terms, e.g. giving the approximate value of 0.01% at $Re = 10^8$. Thus, in a low-disturbance environment such an interaction provides a possible route to transition. Similar reasoning applies to the scales in vortex/TS-wave interactions. Accordingly, much work is in progress on the determination of vortex/wave interactions under various conditions. Yet, although a number of weakly nonlinear interactions have been addressed already (see references above), there appear to be very few firm results so far for strongly nonlinear interactions, and the latter's solution properties and interpretations must still be regarded as largely unknown. This provides the motivation for the current study, which concerns certain exact solutions, their eruptive behaviour, and singularities, among other things.

The applications of vortex/wave interaction theory are believed to be widespread, in addition to those mentioned above, as noted by Hall & Smith (1991) who also review some of the theoretical and practical aspects involved. Again, there are numerous types of strongly nonlinear vortex/wave interaction possible, and the present work applies to many of these in principle. Other strongly nonlinear theories relevant to transition are those of pressure–displacement nonlinear interaction (Smith 1979*a*, *b*, 1989, 1991; Hoyle, Smith & Walker 1991, 1992) and of Euler/high-frequency motions (Smith & Burggraf 1985; Smith & Stewart 1987; Smith, Doorly & Rothmayer 1990), but these arise for higher amplitudes of input typically, although there are connections between the three theories (see also §5 below) in terms of changes of scale with increasing time and/or distance, as reviewed by Smith (1991) for example.

The governing equations consist of a three-dimensional vortex longitudinal system for the unknown mean flow coupled with a three-dimensional TS-type wave equation via an effective surface-slip condition. These are presented in §2 below, which also describes two types of finite-distance singularity that can occur in the solution in the spatial-marching context, cf. the Appendix. Following that, an exact solution of the governing equations of a similarity form is studied in §§3, 4, analytically and computationally respectively, and the results are discussed further, compared and interpreted in §5, where an interesting link between the similarity solutions and the finite-distance singularities of §2 is found to emerge.

The work in §2 is guided by the brief suggestions in Smith & Walton (1989) and

is given in more detail by Walton (1991). The finite-distance singularities proposed are, first, of a lift-off separation type like those considered in other contexts by Sychev (1979), Simpson & Stewartson (1982*a*, *b*), Elliott, Cowley & Smith (1983), Cebeci, Stewartson & Schimke (1984), and others, but in three-dimensions here; and, second, of a strongly attaching-flow type, localized in the spanwise coordinate. The former type is also reconsidered for the temporal-marching context in the Appendix, where a similar lift-off solution behaviour is found. The lift-off separation of the vortex flow is brought about by the tripping action of the surface-slip effect (referred to earlier) which acts in the azimuthal direction; without this slip, i.e. without the wave present, the vortex flow would probably stay attached for most practical starting conditions and approach a two-dimensional state far downstream, in the spatial setting. Locally, the separation singularity in particular is largely independent of the wave pressure–displacement law, with the flow structure here bearing resemblance to the lift-off or eruption of lambda vortices that has been observed experimentally during boundary-layer or channel-flow transition.

The link between §2 and §5 mentioned earlier in this paragraph is that analogous singularities appear to arise in the nonlinear similarity solutions. Further, we observe that spanwise periodicity is imposed for convenience in the nonlinear similarity study (§§3, 4) but this is not necessary in general and in fact the entire nonlinear vortex pattern could move about in the spanwise direction; in line with that, the separation-like and attachment-like singular behaviour possible in the similarity results does not necessarily happen along the particular symmetry lines imposed but in between. Section 5 also discusses the main follow-on from the separation singularity, namely that local nonlinear pressure–displacement interaction with the outer flow enters play next. This inner–outer interaction leads, in the spatial–temporal setting, to the breakup singularity of Smith (1988) and thence to local vortex formation, which Hoyle *et al.* (1991, 1992) associate with the occurrence of the so-called 'first spike' in fully fledged transition (although there are other explanations suggested for this spike). Further, recent comparisons by Smith & Bowles (1992) show close quantitative agreement with the experiments by Nishioka concerning the first spike.

The flow structure for the vortex/TS-wave interaction studied here is given in figure 1, for the boundary-layer case on a flat surface. The velocities (u_n, v_n, w_n), corresponding Cartesian coordinates (x_n, y_n, z_n) (streamwise, normal, spanwise), and time (t_n) are non-dimensionalized with respect to the references values u_{ref}, l_{ref}, l_{ref}/u_{ref}, in turn, the pressure p_n with respect to ρu_{ref}^2, and $Re \equiv u_{ref} l_{ref}/\nu$, where ρ, ν are respectively the density and kinematic viscosity of the fluid, which is assumed incompressible in the present applications. The flow field is multi-structured (Smith & Walton 1989; Hall & Smith 1991), with a mean-flow correction of relative order $(h^{-2}/\ln h)$ present within the $O(Re^{-\frac{5}{8}})$-thick lower deck of the triple-deck structure necessary for the TS wave. Nonlinear forcing by the small-amplitude waves results in the spanwise mean-flow correction growing logarithmically with distance from the surface. This leads to the formation of a buffer zone between the lower deck and the main portion of the $O(Re^{-\frac{1}{8}})$-thick boundary layer. In this buffer zone $y_n = Re^{-\frac{5}{8}}hy$, x_n-constant $= Re^{-\frac{3}{8}}h^3x$, z_n – constant $= Re^{-\frac{3}{8}}z$, and

$$[u_n, v_n, w_n] = [Re^{-\frac{1}{8}}hu, Re^{-\frac{3}{8}}h^{-1}v, Re^{-\frac{1}{8}}h^{-2}w] \tag{1.1}$$

to leading order, with the vortex timescale being $t_n = Re^{-\frac{1}{4}}h^2t$. Here the parameter h lies between $O(1)$ and $O(Re^{\frac{1}{8}})$. If h is reduced to order unity then the full triple-deck nonlinear interaction is provoked, whereas if h is increased to order $Re^{\frac{1}{8}}$ the

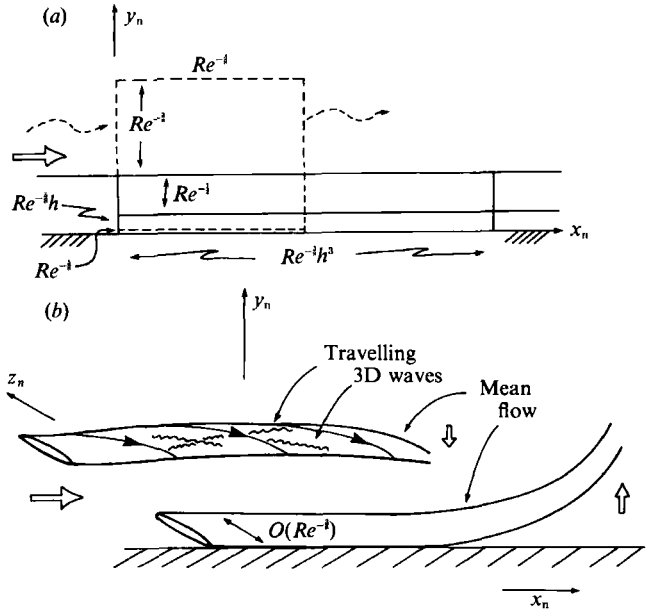

FIGURE 1. Schematic diagram of the flow structure for the vortex/Tollmien–Schlichting interaction. (*a*) Streamwise section showing the travelling three-dimensional TS wave structure (triple deck), in dashed lines, and the main vortex structure which is elongated and involves a buffer region. (*b*) Sketch of the flow (vortex system plus three-dimensional waves), indicating the proposed lift-off separation and the strong attachment downstream: see §§2, 5.

longitudinal vortex motion occupies the whole boundary layer. With $1 \ll h \ll Re^{\frac{1}{8}}$, in contrast, the form (1.1) substituted into the Navier–Stokes equations leads to a vortex system in the buffer zone, as given in the next section.

Along with (1.1), the TS-wave component of the total flow has the three-dimensional triple-deck character, with typical pressure amplitude level p_n of order $Re^{-\frac{1}{8}}h^{-1}$ times a logarithmic factor and timescale of order $Re^{-\frac{1}{4}}$. Nonlinear effects from the wave inertia then produce a forcing constraint proportional to amplitude-squared on the vortex system, in the earlier-noted form of a spanwise slip velocity, in effect, at the bottom of the buffer zone. The corresponding forcing on the wave system occurs through the vortex surface-shear distribution (λ_0 below) which appears in the coefficients of the wave equation, thus inducing strongly nonlinear interaction between the mean-flow vortex and the wave. Similar formulations hold in other applications. The resulting vortex/wave equations are presented in (2.1*a–l*) below, with the scaled vortex shear λ_0 and the scaled wave pressure p and negative displacement A all being unknowns.

2. Vortex/wave interaction equations, and finite-distance singularities

The *vortex* flow is governed by the three-dimensional boundary-layer equations

$$\frac{\partial u}{\partial x}+\frac{\partial v}{\partial y}+\frac{\partial w}{\partial z}=0, \tag{2.1a}$$

$$\frac{\partial u}{\partial t}+u\frac{\partial u}{\partial x}+v\frac{\partial u}{\partial y}+w\frac{\partial u}{\partial z}=\frac{\partial^2 u}{\partial y^2}, \tag{2.1b}$$

$$\frac{\partial w}{\partial t}+u\frac{\partial w}{\partial x}+v\frac{\partial w}{\partial y}+w\frac{\partial w}{\partial z}=\frac{\partial^2 w}{\partial y^2}, \tag{2.1c}$$

together with the boundary conditions

$$\frac{\partial u}{\partial y}\to 1, \quad w\to 0 \quad \text{as} \quad y\to\infty, \tag{2.1d, e}$$

$$\frac{\partial u}{\partial y}\to\lambda_0, \quad w\to -\frac{1}{\alpha^2\lambda_0^2}\left\{\alpha^2\frac{\partial}{\partial z}(pp^*)+\frac{\partial}{\partial z}\left(\frac{\partial p}{\partial z}\frac{\partial p^*}{\partial z}\right)\right\} \quad \text{as} \quad y\to 0 \tag{2.1f, g}$$

and coupled with the TS *wave* pressure equation

$$p_{zz}+\frac{\lambda_{0z}}{\lambda_0}\mathscr{F}(z,x,t)\,p_z-\alpha^2 p=\mathscr{G}(z,x,t)\,\mathscr{H}(p), \tag{2.1h}$$

where the pressure–displacement law has been written in the general form $A=\mathscr{H}(p)$ and the asterisk in (2.1*g*) denotes the complex conjugate. This law can be derived from the solution in the upper deck (where $y=Re^{-\frac{1}{8}}\bar{y}$) of the Helmholtz equation

$$\left.\begin{aligned}&\left(\frac{\partial^2}{\partial\bar{y}^2}+\frac{\partial^2}{\partial z^2}-\alpha^2\right)\bar{p}=0,\\ &\text{subject to the conditions}\\ &\bar{p}=p, \quad \frac{\partial\bar{p}}{\partial\bar{y}}=-\alpha^2\mathscr{H} \quad \text{at} \quad \bar{y}=0+\end{aligned}\right\} \tag{2.1i}$$

and $\bar{p}$ bounded at infinity, in our specific case. The absence of pressure-gradient terms in (2.1*b*, *c*) is because the vortex pressure is found to be negligible at leading order (Smith & Walton 1989). The functions $\mathscr{F}$, $\mathscr{G}$ are defined by

$$\mathscr{F}=-\tfrac{3}{2}-\frac{\xi_0(\xi_0\mathscr{K}(\xi_0)+\mathrm{Ai}'(\xi_0))}{2\mathrm{Ai}(\xi_0)}, \qquad \mathscr{G}=(\mathrm{i}\alpha\lambda_0)^{\frac{5}{3}}\frac{\mathrm{Ai}'(\xi_0)}{\mathscr{K}(\xi_0)}, \tag{2.1j, k}$$

$$\xi_0=-\frac{\mathrm{i}^{\frac{1}{3}}\Omega}{(\alpha\lambda_0)^{\frac{2}{3}}}, \qquad \mathscr{K}(\xi_0)=\int_{\xi_0}^{\infty}\mathrm{Ai}(q)\,\mathrm{d}q, \tag{2.1l, m}$$

where Ai denotes the Airy function and the wavenumber α and the frequency Ω must both be real. Starting conditions, at $x=0$ say for the spatial case ($\partial/\partial t\equiv 0$), are also assumed.

The solution of the vortex/wave interaction system (2.1) is a computational problem in general and a complex and time-consuming one at that (e.g. see Hall & Smith 1991). Extra insight may be gained by examining possibilities for the ultimate downstream form. In this section we consider two such possibilities for the nonlinear interaction with $\partial/\partial t\equiv 0$ in (2.1), both of which take the form of finite-distance singularities (a third which is considered in §3 is found to have connections with the present two). The first of these (§2.1), in which the local flow remains fully three-dimensional, is governed primarily by inviscid dynamics and results in the formation of a relatively large 'separation' region which thickens in singular fashion as some

finite x-station is approached. In this region, the magnitude of the streamwise flow is greatly reduced in comparison with that in the adjacent layers, where the velocity profiles are dependent upon the flow history. In contrast, the second possibility, considered (§2.2), in which the predominant flow is in the cross-stream direction, results in a strong 'attachment' of the boundary layer with the skin friction becoming singular at a finite distance downstream.

For convenience, the work in the rest of this section is in terms of the flow solution near a symmetry line $z = z_0$, where we assume the spanwise velocity to pass through zero, although this can be generalized later (§§3–5). Thus the solutions must assume the local form

$$[u, v, w] = [\bar{u}(x, y), \bar{v}(x, y), (z-z_0)\,\bar{w}(x, y)]\,(1+O(z-z_0)), \tag{2.2a}$$

$$p = \bar{p}_0(x) + (z-z_0)^2\,\bar{p}_2(x) + \ldots, \tag{2.2b}$$

$$\mathscr{H} = \bar{\mathscr{H}}(x) + O(z-z_0). \tag{2.2c}$$

In this case the governing equations above reduce to

$$\frac{\partial \bar{u}}{\partial x} + \frac{\partial \bar{v}}{\partial y} + \bar{w} = 0, \quad \bar{u}\frac{\partial \bar{u}}{\partial x} + \bar{v}\frac{\partial \bar{u}}{\partial y} = \frac{\partial^2 \bar{u}}{\partial y^2}, \tag{2.3a, b}$$

$$\bar{u}\frac{\partial \bar{w}}{\partial x} + \bar{v}\frac{\partial \bar{w}}{\partial y} + \bar{w}^2 = \frac{\partial^2 \bar{w}}{\partial y^2}, \tag{2.3c}$$

with

$$\frac{\partial \bar{u}}{\partial y} \to 1, \quad \bar{w} \to 0 \quad \text{as} \quad y \to \infty, \tag{2.3d, e}$$

$$\frac{\partial \bar{u}}{\partial y} \to \bar{\lambda}_0, \quad \bar{w} \to -\frac{[8|\bar{p}_2|^2 + 2\alpha^2(\bar{p}_0\,\bar{p}_2^* + \text{c.c.})]}{\alpha^2 \bar{\lambda}_0^2} \quad \text{as} \quad y \to 0 \tag{2.3f, g}$$

where c.c. denotes complex conjugation and the TS pressure equation now takes the form

$$2\bar{p}_2 - \alpha^2 \bar{p}_0 = \bar{\mathscr{G}}\bar{\mathscr{H}} \tag{2.3h}$$

($\bar{\mathscr{G}}$ is $\mathscr{G}$ with $\bar{\lambda}_0$ (unknown) replacing λ_0). This system poses a far less formidable problem than the full set (2.1), both computationally and analytically.

2.1. *The finite-distance separation singularity*

An intriguing possibility is that the interaction results in a three-dimensional separation singularity at a finite station $x = x_s$, say, downstream. For simplicity, we consider the flow near a symmetry line as described above, supposing the vortex velocity components (as $x \to x_s -$) to take the form:

$$\bar{u} = (x_s - x)^q F(\bar{y}) + (x_s - x)^{2N+1} F_1(\bar{y}) + \ldots, \tag{2.4a}$$

$$\bar{v} = (x_s - x)^{-\gamma} G(\bar{y}) + (x_s - x)^N G_1(\bar{y}) + \ldots, \tag{2.4b}$$

$$\bar{w} = (x_s - x)^{-\gamma+N} H(\bar{y}) + (x_s - x)^{2N} H_1(\bar{y}) + \ldots, \tag{2.4c}$$

with $y = (x_s - x)^{-N}\,\bar{y}$. The powers shown are to be determined, but we require $q > 0$ to ensure that the flow speed is less than that of the free stream, and q is related to the other constants here via the relation $q = 1 - \gamma + N$. The velocity forms (2.4) adopted here are motivated by the expectation that the three-dimensional flow will remain governed by nonlinear dynamics. We also take the parameter $N > 0$ so that

the flow region undergoes singular thickening as $x \to x_s-$. With the restriction $q > 1-2\gamma$, substitution into the symmetry-line equations (2.3) yields the following nonlinear balances:

$$-qF - N\bar{y}\frac{\mathrm{d}F}{\mathrm{d}\bar{y}} + \frac{\mathrm{d}G}{\mathrm{d}\bar{y}} + H = 0, \tag{2.5a}$$

$$-qF^2 - N\bar{y}F\frac{\mathrm{d}F}{\mathrm{d}\bar{y}} + G\frac{\mathrm{d}F}{\mathrm{d}\bar{y}} = 0, \tag{2.5b}$$

$$-(q-1)FH - N\bar{y}F\frac{\mathrm{d}H}{\mathrm{d}\bar{y}} + G\frac{\mathrm{d}H}{\mathrm{d}\bar{y}} + H^2 = 0, \tag{2.5c}$$

providing an inviscid response at first order. So if the expressions for G, H from (2.5a, b) are inserted in (2.5c), the nonlinear equation

$$q^2\left(F^4\frac{\mathrm{d}^3F}{\mathrm{d}\bar{y}^3}\frac{\mathrm{d}F}{\mathrm{d}\bar{y}} - F^4\left(\frac{\mathrm{d}^2F}{\mathrm{d}\bar{y}^2}\right)^2\right) - (N+q)(1-N-q)F^2\left(\frac{\mathrm{d}F}{\mathrm{d}\bar{y}}\right)^4 + q(1-2N-q)F^3\left(\frac{\mathrm{d}F}{\mathrm{d}\bar{y}}\right)^2\frac{\mathrm{d}^2F}{\mathrm{d}\bar{y}^2} = 0 \tag{2.6}$$

is obtained for F. The substitution $\mu = \mathrm{d}F/\mathrm{d}\bar{y}$ the produces the linear equation

$$q^2\left[F^2\frac{\mathrm{d}^2\mu}{\mathrm{d}F^2} + F\frac{\mathrm{d}\mu}{\mathrm{d}F}\right] + q(1-2N-2q)F\frac{\mathrm{d}\mu}{\mathrm{d}F} - (N+q)(1-N-q)\mu = 0 \tag{2.7}$$

for $\mu(F)$, which has the general solution

$$\mu\left[= \frac{\mathrm{d}F}{\mathrm{d}\bar{y}}\right] = a_1F^{m_1} + a_2F^{m_2}, \tag{2.8}$$

where $m_1 = 1+N/q$, $m_2 = m_1 - 1/q$ and a_1, a_2 are arbitrary constants. The solution depends crucially upon the values of the exponents m_1, m_2 and certain restrictions can be placed on these constants by use of the boundary conditions and other physical considerations. With F governed by (2.8), the velocity components G and H take the form

$$G = \frac{(q/a_1)F^{(1-N/q)}}{1+(a_2/a_1)F^{-1/q}} + N\bar{y}F, \quad H = -\frac{(a_2/a_1)F^{(1-1/q)}}{1+(a_2/a_1)F^{-1/q}}, \tag{2.9a, b}$$

from substitution of (2.8) into (2.5a, b). Thus we see that H remains single-signed throughout the layer provided F is positive. We now examine the behaviour of F at the edges of the layer, as $\bar{y} \to 0+$ and $\bar{y} \to \bar{y}_1-$, say. Assuming that $|F|$ becomes large in these limits, the first two terms in (2.8) dominate, giving

$$F(\bar{y}) \sim (Na_1/q)^{-q/N}(\bar{y}_1 - \bar{y})^{-q/N} \quad \text{as} \quad \bar{y} \to \bar{y}_1- \tag{2.10a}$$

and

$$F(\bar{y}) \sim (-1)^{q/N}(Na_1/q)^{-q/N}\bar{y}^{-q/N}(1+O(\bar{y}^{1/N})) \quad \text{as} \quad \bar{y} \to 0+. \tag{2.10b}$$

Hence the sizes of the velocity components in the adjacent layers can now be deduced. The curved upper layer has $O(1)$ thickness and, from (2.9), (2.10),

$$\bar{u} = \tilde{U}(\tilde{y}) + (x_s - x)\tilde{U}_1(\tilde{y}) + \ldots, \quad \bar{v} = N\bar{y}_1(x_s-x)^{-N-1}\tilde{U}(\tilde{y}) + \ldots + \tilde{V}(\tilde{y}) + \ldots, \tag{2.11a, b}$$

$$\bar{w} = \tilde{W}(\tilde{y}) + (x_s - x)\tilde{W}_1(\tilde{y}) + \ldots, \quad y = \bar{y}_1(x_s-x)^{-N} + \tilde{y}. \tag{2.11c, d}$$

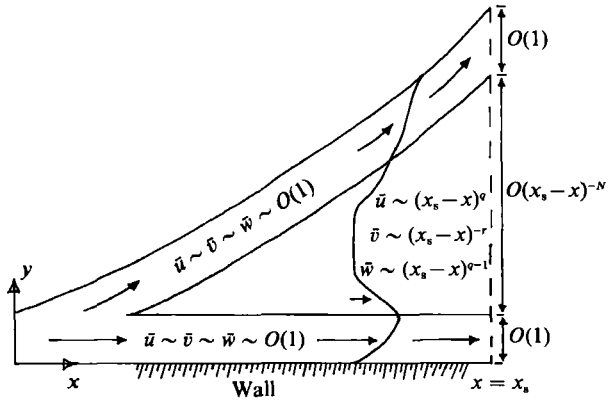

FIGURE 2. The structure of the finite-distance separation singularity in the (x, y)-plane. Note that the $O(1)$ wall layer may be absent in some cases: see text.

Here $\tilde{W} \to 0$, $\mathrm{d}\tilde{U}/\mathrm{d}\tilde{y} \to 1$ as $\tilde{y} \to \infty$, with the latter condition resulting in the effective boundary-layer displacement $-\tilde{A}_{\mathrm{v}}$ growing in the form

$$-\tilde{A}_{\mathrm{v}} \propto (x_{\mathrm{s}}-x)^{-N} \quad \text{as} \quad x \to x_{\mathrm{s}}-. \tag{2.12}$$

Substitution of the expansions (2.11) into the governing equations (2.3*a–c*) yields at leading order the following three equations in five unknowns:

$$-\tilde{U}_1+\tilde{V}'+\tilde{W}=0, \quad -\tilde{U}\tilde{U}_1+\tilde{V}\tilde{U}'=\tilde{U}'', \quad -\tilde{U}\tilde{W}_1+\tilde{V}\tilde{W}'+\tilde{W}^2=\tilde{W}''.$$

This leaves us free to choose two out of $(\tilde{U}, \tilde{V}, \tilde{W})$ although the profiles chosen are required to match with those in the layer underneath and with the outer boundary conditions (2.3*d*, *e*). An $O(1)$ region may also be present near the wall, with the profiles once again possessing some degree of arbitrariness (the flow structure without this extra layer is discussed at the end of this section). In both $O(1)$ regions the leading-order profiles are dependent upon the flow 'history', i.e. they vary according to the starting conditions imposed. In the lower layer, again from (2.9), (2.10),

$$\bar{u} = \hat{U}(\hat{y})+\ldots, \quad \bar{v} = \hat{V}(\hat{y})+\ldots, \quad \bar{w} = \hat{W}(\hat{y})+\ldots, \quad y = \hat{y}, \tag{2.13a–d}$$

with these profiles subject to matching with the wider $O(x_{\mathrm{s}}-x)^{-N}$ middle layer and conditions at the wall, where in particular $\hat{W}$ is subject to the TS pressure forcing. The main features of the flow structure described above are sketched in figure 2.

Concerning the values of q, N, γ, it can be seen from (2.10) that q/N must be an integer. Furthermore, since the approach to the breakdown is from upstream, the streamwise component $\bar{u}$ must be positive, i.e. we are assuming there has been no flow reversal up to this point. Thus we require the condition $F \to \infty$ at both edges of the middle layer, which leads us to the conclusion that q/N must be an even positive integer since this is the only way in which the expressions for F in (2.10*a*, *b*) can both be positive. It then follows that $\mathrm{d}F/\mathrm{d}\bar{y} \to \infty$ at one edge and $\mathrm{d}F/\mathrm{d}\bar{y} \to -\infty$ at the other. So, assuming smoothness, $\mathrm{d}F/\mathrm{d}\bar{y}$ must become zero at some internal point $\bar{y} = \bar{y}_2$ say, and from (2.8) either $F(\bar{y}_2) = 0$ or $F(\bar{y}_2) = (-a_2/a_1)^q$; only the former is acceptable, however, if $\bar{y}_2$ is finite (Walton 1991). Hence the local behaviour is

$$F \sim (a_2)^{q/(1-N)}\,((1-N)/q)^{q/(1-N)}\,(\bar{y}-\bar{y}_2)^{q/(1-N)} \quad \text{as} \quad \bar{y} \to \bar{y}_2 \pm, \tag{2.14}$$

from examination of (2.8) with F assumed small. Since we require the streamwise velocity component to be in the positive x-direction, (2.14) requires $q/(1-N)$ to be

an even positive integer. As the value of $q/(1-N)$ is increased, the streamwise velocity profile in this wide middle layer becomes more rounded around the turning point $\bar{y} = \bar{y}_2$ (compare the curves in figure 4*a*). In general, then, we have:

$$\frac{q}{1-N} = 2L, \quad L = 1,2,3,\ldots; \quad \frac{q}{N} = 2K, \quad K = 1,2,3,\ldots, \tag{2.15a, b}$$

leading to the following values for the relevant parameters:

$$N = \frac{L}{K+L}, \quad q = \frac{2KL}{K+L}, \quad \gamma = \frac{2L+K-2KL}{K+L}, \quad m_1 = \frac{2K+1}{2K}, \quad m_2 = \frac{2L-1}{2L}, \tag{2.16a–e}$$

from which it can be seen that m_1 and m_2 are both positive; see also the limiting cases noted below. However, we have the additional restriction $q > 1-2\gamma$ (used in obtaining (2.5)), which effectively ensures that the viscous effects are only present at higher order. Therefore, $K < 3L/(2L-1)$, so that, for $L = 1$, only $K = 1,2$ are permitted, implying

$$(N,q) = (\tfrac{1}{2},1) \text{ or } (\tfrac{1}{3},\tfrac{4}{3}) \quad (L = 1). \tag{2.17}$$

For $L \geqslant 2$, there is only one possible value for K ($K = 1$) in each case and so the constants take the values

$$N = \frac{L}{1+L}, \quad q = 2N, \quad \gamma = \frac{1}{1+L}, \quad m_1 = \tfrac{3}{2}, \quad m_2 = \frac{2L-1}{2L} \quad (L \geqslant 2). \tag{2.18}$$

The limiting case where $L \to \infty$, $N \to 1-$, $q \to 2-$, $m_2 \to 1-$, $\gamma \to 0+$ is also considered by Walton (1991), while the limiting case where $L \sim K \sim q \to 0$, $(N,\gamma) \to (\frac{1}{2},\frac{3}{2})$, $F \to$ constant and $(2G/F - \bar{y})$, $(2H/F + 1)$ acquire sine, cosine forms respectively, is in line with results by Dr S. N. Timoshin (private communications, 1992). For both of the cases where $L = 1$ it is apparent that the quantity $q/(1-N) = 2$. From (2.14) we see that this choice leads to the second and all higher derivatives of F remaining non-zero at the location where F is zero. We now examine these two cases in more detail.

Example 1 is the case $L = 1, K = 1$ where $N = \frac{1}{2}$, $q = 1$, $\gamma = \frac{1}{2}$, $m_1 = \frac{3}{2}$, $m_2 = \frac{1}{2}$. In this case the middle layer is of $O(x_s - x)^{-\frac{1}{2}}$ thickness, the streamwise velocity is $O(x_s - x)$, smaller than in the adjacent layers, the spanwise velocity is $O(1)$, but the radial component is large, of order $(x_s - x)^{-\frac{1}{2}}$ and the skin-friction response is proportional to $(x_s - x)^{\frac{3}{2}}$. Here (2.8) can be solved analytically for F, giving

$$F = (a_2/a_1)\tan^2(\tfrac{1}{2}(a_1 a_2)^{\frac{1}{2}}(\bar{y} - D)). \tag{2.19}$$

By choosing the constant D to have the value $\pi(a_1 a_2)^{-\frac{1}{2}}$, we can ensure $F \to \infty$ as $\bar{y} \to 0+$, in the approach to the $O(1)$ wall layer. In this case, the zero of F occurs at the value $\bar{y} = \bar{y}_2 = \pi(a_1 a_2)^{-\frac{1}{2}}$ and the upper extreme of the layer is at $\bar{y} = \bar{y}_1 = 2\pi/(a_1 a_2)^{\frac{1}{2}}$, so that F is symmetrical about the zero point (see figure 3*a*, plotted for the case $a_1 = a_2 = 1$). The corresponding expressions for the other components G, H (deduced from (2.9)) are

$$G = \left(\frac{a_2}{a_1}\right)\left\{\tfrac{1}{2}\bar{y} + \frac{1}{(a_1 a_2)^{\frac{1}{2}}}\sin\sigma\cos\sigma\right\}\tan^2\sigma, \tag{2.20a}$$

$$H = -(a_2/a_1)\sin^2\sigma, \quad 2\sigma \equiv (a_1 a_2)^{\frac{1}{2}}\bar{y} - \pi, \tag{2.20b}$$

and these are sketched in figures 3(*b*) and 3(*c*) where once again we have taken $a_1 = a_2 = 1$ for convenience.

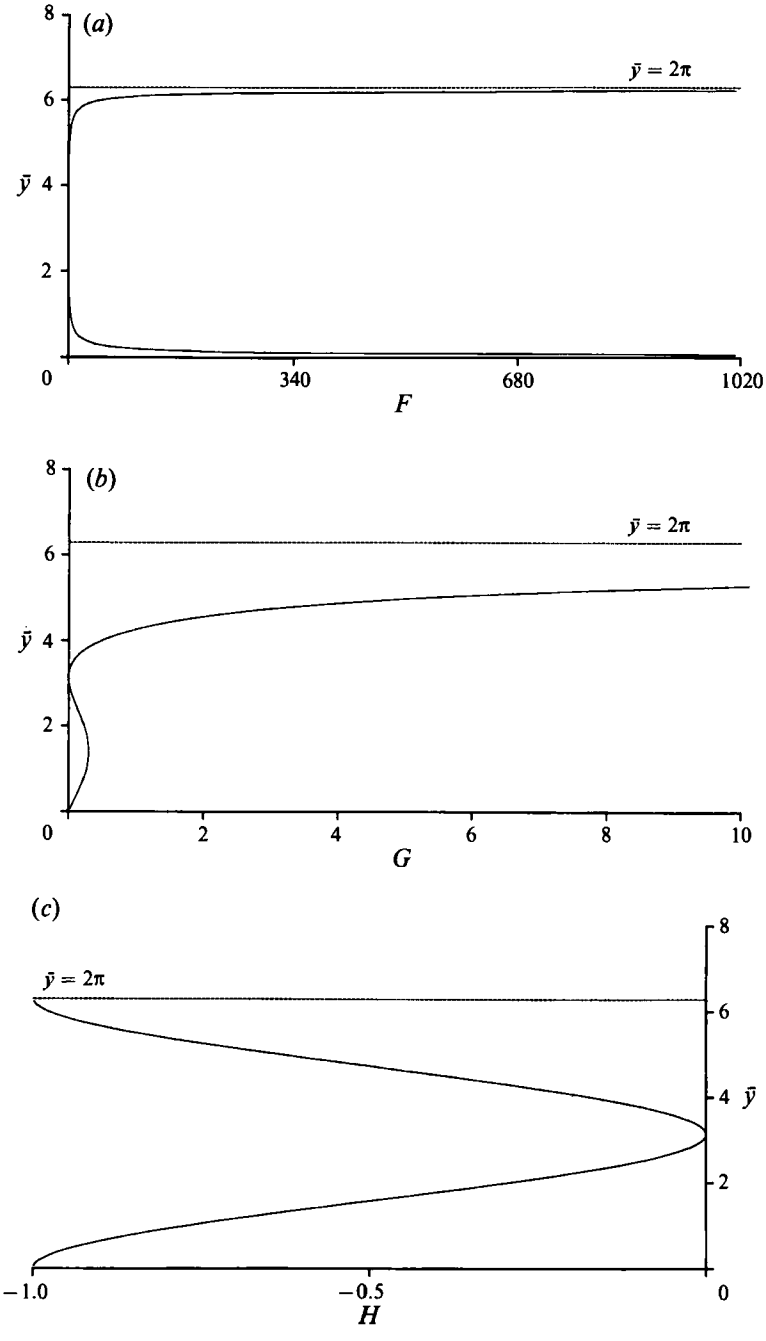

FIGURE 3. Middle-layer velocity profiles for the case $N = \frac{1}{2}$, $q = 1$ (Example 1 of §2), with $a_1 = a_2 = 1$: (*a*) Streamwise velocity $F(\bar{y})$, the curve is described analytically by (2.19). (*b*) Radial velocity $G(\bar{y})$, the curve is described analytically by (2.20*a*). (*c*) Spanwise velocity $H(\bar{y})$, the curve is described analytically by (2.20*b*).

Example 2 has $L = 1$, $K = 2$ and $N = \frac{1}{3}$, $q = \frac{4}{3}$, $\gamma = 0$, $m_1 = \frac{5}{4}$ and $m_2 = \frac{1}{2}$. Here, as in all cases, the streamwise velocity is smaller than in the adjacent layers, with the skin-friction response now proportional to $(x_s - x)^{\frac{5}{3}}$. Also, the spanwise velocity is small, $O(x_s - x)^{\frac{1}{3}}$, and the radial velocity is $O(1)$ because $\gamma = 0$. Overall then, the flow

velocities in this layer, which is of $O(x_s-x)^{-\frac{1}{3}}$ thickness, are less than in the previous example, although the velocity profiles are similar in shape. In this case the equation for the shear takes the form

$$\mathrm{d}F/\mathrm{d}\bar{y} = a_1 F^{\frac{5}{4}} + a_2 F^{\frac{1}{2}}, \tag{2.21}$$

the solution of which is (with $\beta_1 = (a_2/a_1)^{\frac{1}{3}}$)

$$\bar{y} = \frac{8\pi}{3\sqrt{3}a_1\beta_1} \pm \left[\frac{2\pi}{3\sqrt{3}a_1\beta_1} - \frac{4}{3a_1\beta_1}\left\{\tfrac{1}{2}\ln\left|\frac{(h+\beta_1)^2}{h^2-\beta_1 h+\beta_1^2}\right| - \sqrt{3}\tan^{-1}\left(\frac{2h-\beta_1}{\beta_1\sqrt{3}}\right)\right\}\right], \quad F = h^4, \tag{2.22}$$

in implicit form, when the correct matching conditions are imposed. So F is zero at $\bar{y} = \bar{y}_2 = 8\pi/3\sqrt{3}a_1\beta_1$, the upper extreme of the layer lies at $\bar{y} = \bar{y}_1 = 16\pi/3\sqrt{3}a_1\beta_1$, and a symmetric profile is obtained, as sketched in figure 4(*a*) with $a_1 = a_2 = 1$ (the inner curve). The similarity with the F profile of Example 1 (figure 3*a*) is evident: since m_2 is the same for both cases, the behaviour of F in the vicinity of $\bar{y} = \bar{y}_2$ is identical. It is only as F increases to match with the larger $O(1)$ velocities in the upper and lower layers that the profiles begin to differ, with F increasing more rapidly in Example 1 owing to the larger value of m_1 there. However, it must be stressed that the actual layer thickness is much greater in Example 1 since the value of N is larger, and so the velocity profile is stretched out much more in this case, as can be seen from the figures. Sketches of the corresponding G, H profiles for Example 2 are shown in figures 4(*b*) and 4(*c*) and it can be seen that they both remain single-signed.

It may be noted that Example 2 is a special case and in fact all the other possibilities ($L \geqslant 2$) bear great similarity to Example 1. For these cases we can write the shear equation in the form

$$\mathrm{d}F/\mathrm{d}\bar{y} = a_1 F^{\frac{3}{4}} + a_2 F^{(2m-3)/2(m-1)}, \tag{2.23}$$

where $m = 2, 3, 4, \ldots$, and this equation is the governing one for all the possibilities apart from that of Example 2. Example 1 corresponds to the case $m = 2$. The appropriate solution of (2.23) is

$$\bar{y} = \frac{2(m-1)}{a_2}\left(\frac{a_2}{a_1}\right)^{1/m}\left(\frac{\pi}{m}\operatorname{cosec}\left(\frac{\pi}{m}\right) \pm \int_0^s \frac{\mathrm{d}s}{1+s^m}\right)$$

with

$$F = (a_2/a_1)^{2(m-1)/m} s^{2(m-1)}. \tag{2.24}$$

The corresponding values of the parameters N, q, γ are

$$N = 1-1/m, \quad q = 2N, \quad \gamma = 1/m, \tag{2.25}$$

leading to a skin-friction response proportional to $(x_s-x)^{3-3/m}$. Thus as m increases, N increases (the middle-layer width increases), q increases (the streamwise and spanwise velocities decrease) and γ decreases (radial velocity reduces to $O(1)$), and the skin friction tends to zero more rapidly. The zero of F occurs at

$$\bar{y} = \bar{y}_2 = \frac{2\pi}{a_2}\left(\frac{m-1}{m}\right)\left(\frac{a_2}{a_1}\right)^{1/m}\operatorname{cosec}\left(\frac{\pi}{m}\right),$$

and F is symmetrical about this zero point. The F-profile for the case $m = 3$ is shown in figure 4(*a*) (the outer curve) with $a_1 = a_2 = 1$ without loss of generality.

Up to this point, we have assumed the existence of an $O(1)$ wall layer in which the TS effects (if any) to some extent determine the nature of the flow locally. The inviscid middle layer is free from these effects and so the influence of the vortex–TS

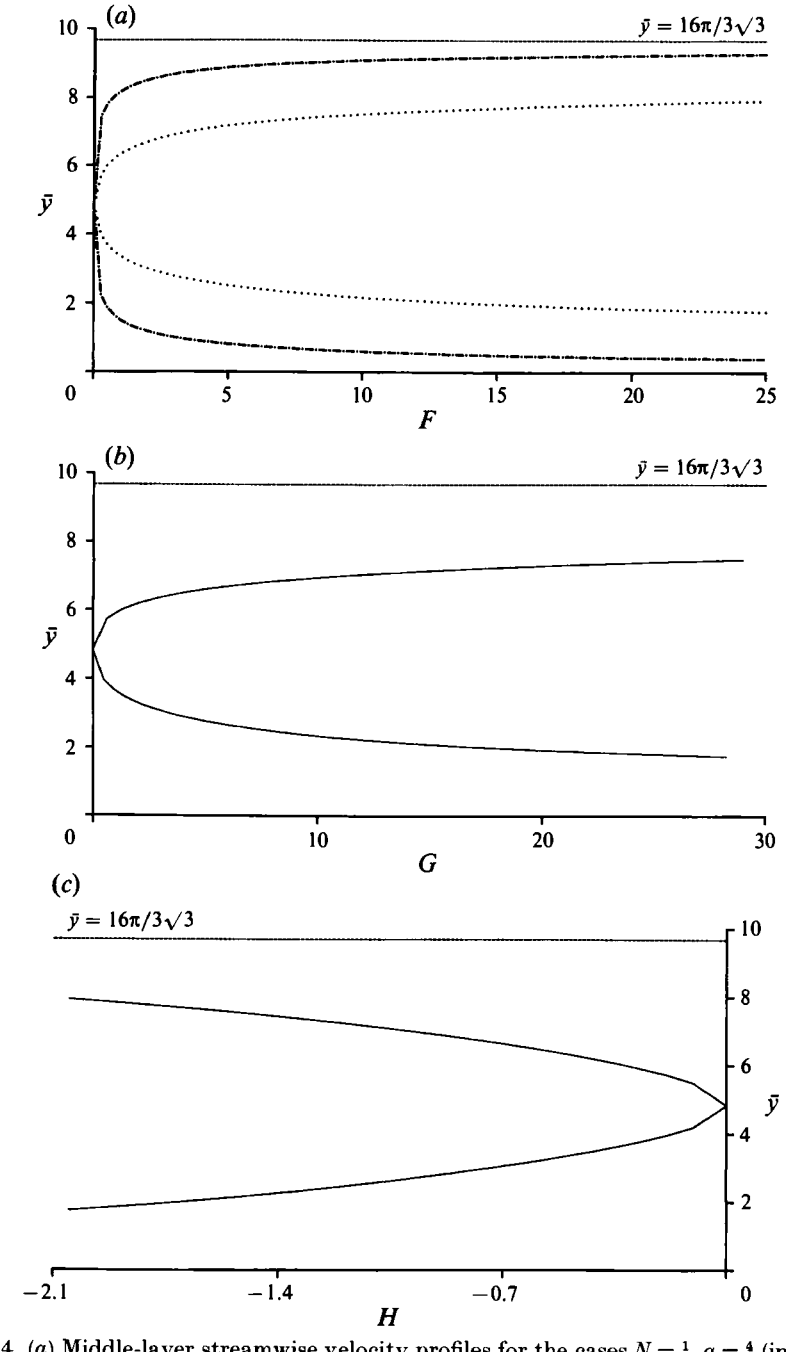

FIGURE 4. (*a*) Middle-layer streamwise velocity profiles for the cases $N = \frac{1}{3}$, $q = \frac{4}{3}$ (inner curve) and $N = \frac{2}{3}$, $q = \frac{4}{3}$ (outer curve) (Example 2 of §2). The inner curve is given analytically by (2.22) with $a_1 = a_2 = 1$. (*b*, *c*) Middle-layer (*b*) radial and (*c*) spanwise velocity profiles for the case $N = \frac{1}{3}$, $q = \frac{4}{3}$ (Example 2 of §2).

interaction is necessarily weak overall, and indeed this finite-distance separation could occur even in the absence of the TS waves. If the wall layer is absent, and in effect this middle layer is directly adjacent to the wall, the expansions in the buffer zone are as in (2.4) with $q = 1-N$ from (2.14) with $\bar{y}_2$ replaced by zero in effect, and

hence $\gamma = 2N$. Thus the shear equation for F now takes the form $\mathrm{d}F/\mathrm{d}\bar{y} = a_1 F^{1/q} + a_2$, so that F is regular only if $1/q$ is a positive integer $m(\geqslant 2)$. The general solution for $\bar{y}(F)$ is then

$$\bar{y} = \frac{1}{a_2}\left(\frac{a_2}{a_1}\right)^{1/m} \int_0^f \frac{\mathrm{d}q}{1+q^m}, \quad m = 2, 3, 4\ldots, \tag{2.26}$$

with $f = (a_1/a_2)^{1/m} F$. The TS forcing affects the second-order terms (F_1, G_1, H_1) in expansions (2.4). This type of structure possesses a lesser degree of arbitrariness than when the extra $O(1)$ layer is present. In particular, it gives very definite predictions for the x-dependence of the vortex skin friction ($\propto (x_s - x)$) and the TS wavenumber ($\propto (x_s - x)^{-1}$). Also the TS pressure amplitude is predicted to decrease like $(x_s - x)^{N+2}$ (with $N = 1 - 1/m$ for $m = 2, 3, 4, \ldots$) as the wavenumber increases, and in principle this feature should be relatively easy to observe in space-marching calculations (cf. Hall & Smith 1991, and comments at the end of this section) if this flow structure does indeed develop.

2.2. *The finite-distance attachment singularity*

The second option concerns the possibility that a strong attachment takes place in the flow at a finite $x(= x_0$, say) downstream. Once again we consider the flow near a symmetry line $z = z_0$. In this situation the flow velocities assume the form

$$\bar{u} = F_0(Y) + \ldots, \quad \bar{v} = (x_0 - x)^{-A} G_0(Y) + \ldots, \quad \bar{w} = (x_0 - x)^{-2A} H_0(Y) + \ldots, \tag{2.27a–c}$$

$$y = (x_0 - x)^A Y, \tag{2.27d}$$

as $x \to x_0-$, with the exponent A satisfying $A > \frac{1}{2}$. So the cross-stream flow (originating from the G_0, H_0 terms) dominates, with the nonlinear balances

$$\frac{\mathrm{d}G_0}{\mathrm{d}Y} + H_0 = 0, \quad G_0 \frac{\mathrm{d}F_0}{\mathrm{d}Y} = \frac{\mathrm{d}^2 F_0}{\mathrm{d}Y^2}, \quad G_0 \frac{\mathrm{d}H_0}{\mathrm{d}Y} + H_0^2 = \frac{\mathrm{d}^2 H_0}{\mathrm{d}Y^2} \tag{2.28a–c}$$

holding, from substitution of (2.27) into the symmetry-line equations. The appropriate solution has

$$F_0 = \frac{1}{B}(\mathrm{e}^{1-\mathrm{e}^{-BY}} - 1), \quad G_0 = B(\mathrm{e}^{-BY} - 1), \quad H_0 = B^2 \mathrm{e}^{-BY}, \tag{2.29a–c}$$

where $B > 0$. From (2.29), the skin-friction response is of the singular form

$$\bar{\lambda}_0 \propto (x_0 - x)^{-A} \quad \text{as} \quad x \to x_0. \tag{2.30}$$

Thus, to satisfy the spanwise slip condition, the TS pressure must become singular also, acquiring the dependence

$$\bar{p}_0 \sim \bar{p}_2 \propto (x_0 - x)^{-2A} \quad \text{as} \quad x \to x_0, \tag{2.31}$$

with the TS wavenumber α remaining $O(1)$; we see therefore that the constant B must satisfy the relation

$$B^2 = -\frac{8|\bar{p}_2|^2 + 2\alpha^2(\bar{p}_0 \bar{p}_2^* + \text{c.c.})}{\alpha^2 \bar{\lambda}_0^2} \tag{2.32}$$

from (2.29c), (2.3g). In (2.32), the x-dependence has been removed so that the pressure and skin-friction terms are now constants. Here, since H_0 is positive, the spanwise flow is directed away from the symmetry line $z = z_0$, and from (2.29c) the radial component is negative, indicating that fluid is being forced towards the wall (figure 5); both components grow in strength as $x \to x_0$.

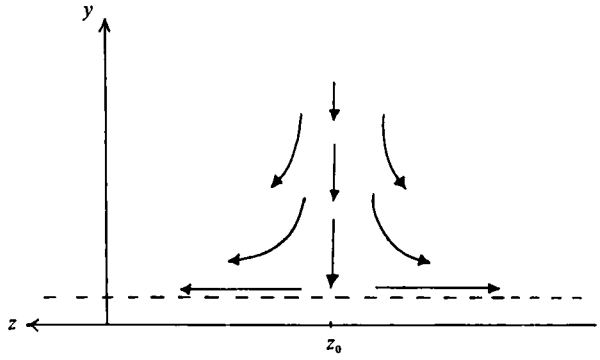

FIGURE 5. The form of the finite-distance attachment singularity in the (y, z)-plane.

It will be interesting to see whether either (or both) of the canonical forms described in this section are observed in further numerical computations of the full space-marching governing equations. Computations for the interaction in an external boundary-layer flow (Hall & Smith 1991) tend to suggest a singularity occurring at a finite distance with, in particular, rapid growth of the TS wavenumber α being observed. Recalling the growth of α predicted earlier, comparisons could be drawn between Hall & Smith's numerical singularity and the lift-off behaviour of §2.1, but more computations need to be performed with a greater number of Fourier modes before any firm conclusions can be drawn on this subject. See also the comparisons in §5 below, however. Again, recent computations by Dr S. N. Timoshin point quite firmly to the proposed lift-off behaviour, in particular for the case $q \to 0$ mentioned earlier.

Flow separation and attachment structures analogous with those described in this section are also possible for the case where the vortex flow possesses time-dependence, and these finite-time singularities are discussed in the Appendix.

3. The similarity form, and some analytical properties

In the similarity form the velocities are expressed as

$$u = x^{\frac{1}{3}}U(\eta, z), \quad v = x^{-\frac{1}{3}}V(\eta, z), \quad w = x^{-\frac{2}{3}}W(\eta, z), \tag{3.1a–c}$$

with $\eta = y/x^{\frac{1}{3}}$ of $O(1)$, yielding an exact solution of the system (2.1) with once again, $\partial/\partial t \equiv 0$ in (2.1a–c). Although strictly valid for all x, this form seems more likely to be acquired downstream, as the effects of the particular starting conditions become less significant. The quantities U, V and W then satisfy the nonlinear equations

$$\tfrac{1}{3}U - \tfrac{1}{3}\eta\frac{\partial U}{\partial \eta} + \frac{\partial V}{\partial \eta} + \frac{\partial W}{\partial z} = 0, \quad \tfrac{1}{3}U^2 - \tfrac{1}{3}\eta U\frac{\partial U}{\partial \eta} + V\frac{\partial U}{\partial \eta} + W\frac{\partial U}{\partial z} = \frac{\partial^2 U}{\partial \eta^2}, \tag{3.2a, b}$$

$$-\tfrac{2}{3}UW - \tfrac{1}{3}\eta U\frac{\partial W}{\partial \eta} + V\frac{\partial W}{\partial \eta} + W\frac{\partial W}{\partial z} = \frac{\partial^2 W}{\partial \eta^2}. \tag{3.2c}$$

In addition, (2.1) suggests writing

$$\lambda_0 = \lambda(z), \quad p = x^{-\frac{1}{3}}P(z), \quad \mathscr{H} = x^{-\frac{1}{3}}\mathscr{H}_s(P). \tag{3.3a–c}$$

Note here that the x-dependence of p in (3.3b) is necessary in order to maintain the effect of the wave on the vortex via (2.1g). The form for $\mathscr{H}$ in (3.3c) then follows

straight from (2.1*i*), with the wavenumber α independent of x at leading order (in fact (3.3*b*, *c*) also apply for compressible boundary layers, jets, channel flows, and so on). The boundary conditions on (3.2) take the form

$$\frac{\partial U}{\partial \eta} \to \lambda(z), \quad W \to -Q(z) \quad \text{as} \quad \eta \to 0+, \quad \frac{\partial U}{\partial \eta} \to 1, \quad W \to 0 \quad \text{as} \quad \eta \to \infty, \tag{3.4a–d}$$

with $\lambda(z)$ unknown, where Q is given by

$$Q = \frac{1}{\alpha^2 \lambda^2}\left\{\alpha^2 \frac{\mathrm{d}}{\mathrm{d}z}(PP^*) + \frac{\mathrm{d}}{\mathrm{d}z}\left(\frac{\mathrm{d}P}{\mathrm{d}z}\frac{\mathrm{d}P^*}{\mathrm{d}z}\right)\right\}, \tag{3.5}$$

and the TS pressure equation is, in general form,

$$P'' + \frac{\lambda'}{\lambda}\mathscr{F}_{\mathrm{s}}(z)\,P' - \alpha^2 P = \mathscr{G}_{\mathrm{s}}(z)\,\mathscr{H}_{\mathrm{s}}(P). \tag{3.6}$$

Here $\mathscr{F}_{\mathrm{s}}, \mathscr{G}_{\mathrm{s}}$ are defined in the same way as $\mathscr{F}, \mathscr{G}$ in §2 except that λ_0 is replaced by λ, so that the x-dependence has been removed (but see also §5 below). The prime in (3.6) denotes differentiation with respect to z. Numerical solutions of the above system are described in §4 below, but before discussing them we consider for guidance certain linear and nonlinear properties.

As a start, an exact solution is the uniform shear flow $U = \eta$, $V = W = 0$, $P =$ constant. So, for small perturbations,

$$U = \eta + \epsilon u_{\mathrm{n}}(\eta)\cos n\beta z + \ldots, \quad V = \epsilon v_{\mathrm{n}}(\eta)\cos n\beta z + \ldots,$$
$$W = \epsilon w_{\mathrm{n}}(\eta)\sin n\beta Z + \ldots, \tag{3.7a–c}$$
$$P = p_0 + \epsilon p_{\mathrm{n}}\cos n\beta z + \ldots, \quad \mathscr{H}_{\mathrm{s}} = \bar{\mathscr{H}} + \epsilon \mathscr{H}_{\mathrm{n}}\cos n\beta z, \tag{3.7d, e}$$

where the spanwise wavenumber n is an integer, and $\epsilon \ll 1$.

Substitution into the vortex equations (3.2) then provides the linear viscous balances

$$\tfrac{1}{3}u_{\mathrm{n}} - \tfrac{1}{3}\eta\frac{\mathrm{d}u_{\mathrm{n}}}{\mathrm{d}\eta} + \frac{\mathrm{d}v_{\mathrm{n}}}{\mathrm{d}\eta} + n\beta w_{\mathrm{n}} = 0, \quad \tfrac{1}{3}\eta u_{\mathrm{n}} - \tfrac{1}{3}\eta^2\frac{\mathrm{d}u_{\mathrm{n}}}{\mathrm{d}\eta} + v_{\mathrm{n}} = \frac{\mathrm{d}^2 u_{\mathrm{n}}}{\mathrm{d}\eta^2}, \tag{3.8a, b}$$

$$-\tfrac{2}{3}\eta w_{\mathrm{n}} - \tfrac{1}{3}\eta^2\frac{\mathrm{d}w_{\mathrm{n}}}{\mathrm{d}\eta} = \frac{\mathrm{d}^2 w_{\mathrm{n}}}{\mathrm{d}\eta^2}. \tag{3.8c}$$

The general solution, with $\chi \equiv \frac{1}{6}\eta^3$, has

$$w_{\mathrm{n}} = -Q_{\mathrm{n}}\,\mathrm{e}^{-2\chi/3} + K\,\mathrm{e}^{-2\chi/3}\int_0^{\chi} s^{-2/3}\,\mathrm{e}^{2s/3}\,\mathrm{d}s, \tag{3.9}$$

where K is arbitrary, and the constant Q_{n} is defined by the expansion for the spanwise slip velocity $Q = \epsilon Q_{\mathrm{n}}\sin n\beta z + \ldots$. By demanding that the velocity w_{n} tends to zero in an exponential rather than algebraic manner (since otherwise the latter would be present for all x), we can neglect the second term in (3.9). Then (3.8*a*, *b*) yield the equation $\mathrm{d}^2 u_{\mathrm{n}}/\mathrm{d}\eta^2 = (n\beta Q_{\mathrm{n}}\eta + D_{\mathrm{n}})\exp(-\frac{1}{9}\eta^3)$. The no-slip condition in (3.8*b*) then implies that $D_{\mathrm{n}} \equiv 0$, while the outer condition requires the shear correction $\mathrm{d}u_{\mathrm{n}}/\mathrm{d}\eta$ to vanish at infinity. Hence upon integration

$$u_{\mathrm{n}} = \left[-3^{\frac{1}{3}}\Gamma(\tfrac{2}{3})\,\eta + 3(\mathrm{e}^{-\eta^3/9} - 1) + \eta\int_0^{\eta} s\,\mathrm{e}^{-s^3/9}\,\mathrm{d}s\right] n\beta Q_{\mathrm{n}}, \quad v_{\mathrm{n}} = n\beta Q_{\mathrm{n}}\,\eta, \tag{3.10a, b}$$

where Γ is the gamma function. The resulting skin friction λ has the form

$$\lambda = 1 - \epsilon 3^{\frac{1}{3}}\Gamma(\tfrac{2}{3})\, n\beta Q_{\rm n} \cos n\beta z + \ldots. \tag{3.11}$$

In addition to being used for comparisons later in the paper, applications of the above to pipe entry flow are considered by Walton (1991).

Another starting solution is $p_0 = \mathscr{H} = 0$, however, with both the TS pressure and displacement then reduced to $O(\epsilon)$. In this case, the TS wave forces a vortex motion at $O(\epsilon^2)$ and the velocities take the form

$$U = \eta + \epsilon^2\left(-3^{\frac{1}{3}}\Gamma(\tfrac{2}{3})\,\eta + 3(\mathrm{e}^{-\eta^3/9} - 1) + \eta\int_0^\eta s\,\mathrm{e}^{-s^3/9}\,\mathrm{d}s\right) 2n\beta\tilde{Q}_{\rm n}\cos 2n\beta z + \ldots, \tag{3.12a}$$

$$V = \epsilon^2 2n\beta\tilde{Q}_{\rm n}\,\eta\cos 2n\beta z + \ldots, \quad W = -\epsilon^2\tilde{Q}_{\rm n}\,\mathrm{e}^{-\eta^3/9}\sin 2n\beta z + \ldots, \tag{3.12b, c}$$

where $\tilde{Q}_{\rm n} = n\beta((n\beta)^2 - \alpha^2)/\alpha^2$. The most notable change from the solution with $O(1)$ TS pressure, apart from the reduction in size of the velocities, is the doubling of the spanwise wavenumber. The appropriate relation linking the frequency and wavenumber to the distance downstream is discussed by Walton (1991), along with other points for entry flow.

Next, we address the symmetry-line version of the similarity solution. A considerable simplification can be made by considering the flow near a symmetry line $z = z_0$, say (cf. §2), where

$$[U, V, W, P] = [\bar{U}(\eta), \bar{V}(\eta), (z - z_0)\,\bar{W}(\eta), \bar{P}_0 + (z - z_0)^2\bar{P}_2][1 + O(z - z_0)], \tag{3.13a}$$

$$\mathscr{G}_{\rm s} = \bar{\mathscr{G}}_{\rm s} + O(z - z_0), \quad \mathscr{H}_{\rm s} = \bar{\mathscr{H}}_{\rm s} + O(z - z_0) \tag{3.13b, c}$$

for $z - z_0 \ll 1$. The vortex equations (3.2) yield here the nonlinear ordinary differential equations

$$\tfrac{1}{3}\bar{U} - \tfrac{1}{3}\eta\frac{\mathrm{d}\bar{U}}{\mathrm{d}\eta} + \frac{\mathrm{d}\bar{V}}{\mathrm{d}\eta} + \bar{W} = 0, \quad \tfrac{1}{3}\bar{U}^2 - \tfrac{1}{3}\eta\bar{U}\frac{\mathrm{d}\bar{U}}{\mathrm{d}\eta} + \bar{V}\frac{\mathrm{d}\bar{U}}{\mathrm{d}\eta} = \frac{\mathrm{d}^2\bar{U}}{\mathrm{d}\eta^2}, \tag{3.14a, b}$$

$$-\tfrac{2}{3}\bar{U}\bar{W} - \tfrac{1}{3}\eta\bar{U}\frac{\mathrm{d}\bar{W}}{\mathrm{d}\eta} + \bar{V}\frac{\mathrm{d}\bar{W}}{\mathrm{d}\eta} + \bar{W}^2 = \frac{\mathrm{d}^2\bar{W}}{\mathrm{d}\eta^2}, \tag{3.14c}$$

subject to the boundary conditions (with $\bar{\lambda}$ unknown)

$$\frac{\partial\bar{U}}{\partial\eta} \to \bar{\lambda}, \quad \bar{W} \to -\bar{Q} \quad \text{as} \quad \eta \to 0+, \quad \frac{\mathrm{d}\bar{U}}{\mathrm{d}\eta} \to 1, \quad \bar{W} \to 0 \quad \text{as} \quad \eta \to \infty. \tag{3.15a–d}$$

Here the spanwise slip velocity $\bar{Q}$ is related to the TS pressure via

$$\bar{Q} = \frac{8|\bar{P}_2|^2 + 2\alpha^2(\bar{P}_0\bar{P}_2^* + \text{c.c.})}{\alpha^2\bar{\lambda}^2}, \tag{3.16}$$

and the pressure terms $\bar{P}_0, \bar{P}_2$ are related by the symmetry-line version of the TS pressure equation:

$$2\bar{P}_2 - \alpha^2\bar{P}_0 = \bar{\mathscr{G}}_{\rm s}\bar{\mathscr{H}}_{\rm s}. \tag{3.17}$$

The vortex equations (3.14) with boundary conditions (3.15) constitute a numerical problem that can be solved relatively easily using a fourth-order Runge–Kutta scheme, as follows. We rescale

$$\bar{U} = \bar{\lambda}^{\frac{2}{3}}\hat{u}(\hat{\eta}), \quad \bar{V} = \bar{\lambda}^{\frac{1}{3}}\hat{v}(\hat{\eta}), \quad \bar{W} = \bar{\lambda}^{\frac{2}{3}}\hat{w}(\hat{\eta}), \quad \bar{Q} = \bar{\lambda}^{\frac{2}{3}}\hat{Q}, \quad \eta = \bar{\lambda}^{-\frac{1}{3}}\hat{\eta}, \tag{3.18a–e}$$

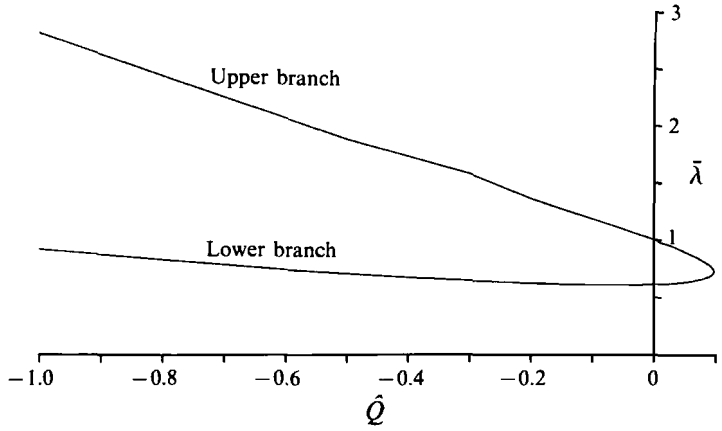

FIGURE 6. Plot of induced vortex skin friction $\bar{\lambda}$ versus spanwise slip velocity $-\hat{Q}$ for the symmetry-line similarity solution of the vortex–wave interaction equations (§3).

after which the vortex equations remain unchanged but now the accompanying boundary conditions are

$$\frac{\mathrm{d}\hat{u}}{\mathrm{d}\hat{\eta}} = 1, \quad \hat{u} = \hat{v} = 0, \quad \hat{w} = -\hat{Q} \quad \text{at} \quad \hat{\eta} = 0; \quad \frac{\mathrm{d}\hat{u}}{\mathrm{d}\hat{\eta}} \to \frac{1}{\bar{\lambda}}, \quad \hat{w} \to 0 \quad \text{as} \quad \hat{\eta} \to \infty. \tag{3.19a–e}$$

Thus we now have an initial-value problem in which we can specify $\hat{Q}$ and iterate upon the value of $\mathrm{d}\hat{w}/\mathrm{d}\hat{\eta}$ at $\hat{\eta} = 0$ in order to make $\hat{w}$ vanish at infinity. For each value of $\hat{Q}$, therefore, there corresponds a value of $\bar{\lambda}$ (not necessarily unique) which can be deduced from the outer conditions. The results of this computation are presented in figure 6, from which it can be seen that no solutions could be found for spanwise slip velocities $\hat{Q} \geqslant \hat{Q}_0$, where $\hat{Q}_0 \approx 0.097$. Also, the region of the curve around the point $\bar{\lambda} = 1$, $\hat{Q} = 0$ can be described by a linear perturbation to the basic shear flow $\hat{u} = \hat{\eta}$, giving

$$\bar{\lambda} = 1 - 3^{\frac{1}{3}}\Gamma(\tfrac{2}{3})\,\hat{Q} \quad \text{for} \quad \hat{Q} \ll 1, \tag{3.20}$$

cf. above. In addition, the numerical results indicate two solutions for $\bar{\lambda}$ for a given $\hat{Q}$, corresponding to differing values of $\mathrm{d}\hat{w}/\mathrm{d}\hat{\eta}$ at $\hat{\eta} = 0$ which both give the required decay in $\hat{w}$ at infinity. It is interesting that this non-uniqueness includes the case of no wave forcing, $\hat{Q} = 0$. Further, as $\hat{Q} \to -\infty$ there are two distinct branches on which $\bar{\lambda} \to \infty$, as described below.

First we tackle the upper branch, where the approach to infinity is more rapid. The flow structure there comprises an inner nonlinear viscous region and a much wider nonlinear inviscid outer one. The inner region has thickness $O(\bar{\lambda}^{-\frac{1}{3}})$ and

$$[\hat{u}, \hat{v}, \hat{w}, \hat{Q}] = [\bar{\lambda}^{-\frac{1}{3}}\tilde{u}, \bar{\lambda}^{\frac{1}{3}}\tilde{v}, \bar{\lambda}^{\frac{2}{3}}\tilde{w}, \bar{\lambda}^{\frac{2}{3}}\tilde{Q}] + \ldots, \quad \hat{\eta} = \bar{\lambda}^{-\frac{1}{3}}\tilde{\eta}, \tag{3.21a–e}$$

so that the vortex flow is governed by

$$\frac{\mathrm{d}\tilde{v}}{\mathrm{d}\tilde{\eta}} + \tilde{w} = 0, \quad \tilde{v}\frac{\mathrm{d}\tilde{u}}{\mathrm{d}\tilde{\eta}} = \frac{\mathrm{d}^2\tilde{u}}{\mathrm{d}\tilde{\eta}^2}, \quad \tilde{v}\frac{\mathrm{d}\tilde{w}}{\mathrm{d}\tilde{\eta}} + \tilde{w}^2 = \frac{\mathrm{d}^2\tilde{w}}{\mathrm{d}\tilde{\eta}^2}. \tag{3.22a–c}$$

The outer conditions in (3.19) apply to the outer inviscid region. The appropriate solution of (3.22) is

$$\tilde{u} = \frac{1}{\gamma_0}(\exp(1 - \mathrm{e}^{-\gamma_0\tilde{\eta}}) - 1), \quad \tilde{v} = \gamma_0(\mathrm{e}^{-\gamma_0\tilde{\eta}} - 1), \quad \tilde{w} = \gamma_0^2\mathrm{e}^{-\gamma_0\tilde{\eta}}, \tag{3.23a–c}$$

where $\gamma_0^2 = -\tilde{Q} > 0$ is a constant to be found. In the outer region, of thickness $O(\bar{\lambda}^{\frac{2}{3}})$, therefore

$$[\hat{u}, \hat{v}, \hat{w}] = [\bar{\lambda}^{-\frac{1}{3}}u^*, \bar{\lambda}^{\frac{1}{3}}v^*, \bar{\lambda}^{-\frac{1}{3}}w^*] + \ldots, \quad \hat{\eta} = \bar{\lambda}^{\frac{2}{3}}\eta^*, \tag{3.24a–d}$$

with the flow velocities satisfying the inviscid balances

$$\tfrac{1}{3}u^* - \tfrac{1}{3}\eta^* u^{*\prime} + v^{*\prime} + w^* = 0, \quad \tfrac{1}{3}u^{*2} - \tfrac{1}{3}\eta^* u^* u^{*\prime} + v^* u^{*\prime} = 0, \tag{3.25a, b}$$

$$-\tfrac{2}{3}u^* w^* - \tfrac{1}{3}\eta^* u^* w^{*\prime} + v^* w^{*\prime} + w^{*2} = 0, \tag{3.25c}$$

with the prime denoting differentiating with respect to η^*. The appropriate matching conditions with the inner region are $u^*(0) = (\mathrm{e}-1)/\gamma_0$, $v^*(0) = -\gamma_0$, while at the outer extremes the boundary conditions require $u^{*\prime}(\infty) = 1$, $w^*(\infty) = 0$. Now, using expressions for v^*, w^* in terms of u^* from (3.25*a*, *b*), the spanwise momentum balance (3.25*c*) results in the nonlinear equation

$$4u^{*3}u^{*\prime\prime}u^{*\prime 2} + u^{*4}u^{*\prime\prime\prime}u^{*\prime} - u^{*4}u^{*\prime\prime 2} = 0 \tag{3.26}$$

for $u^*(\eta^*)$. The substitution $\mathscr{P} = u^{*\prime}$, however, reduces (3.26) to the linear equation $u^* \mathrm{d}^2\mathscr{P}/\mathrm{d}u^{*2} + 4\mathrm{d}\mathscr{P}/\mathrm{d}u^* = 0$, the appropriate solution being

$$\mathscr{P} = \mathrm{d}u^*/\mathrm{d}\eta^* = 1 - a_0^3/u^{*3} \tag{3.27}$$

in view of the outer conditions. Here a_0 is an unknown constant. The implicit solution for $u^*(\eta^*)$ is therefore

$$\eta^* + K_0 = u^* + \tfrac{1}{3}a_0\left[\ln\left|\frac{u^* - a_0}{(u^{*2} + a_0 u^* + a_0^2)^{\frac{1}{2}}}\right| - \sqrt{3}\tan^{-1}\left\{\frac{2u^* + a_0}{a_0\sqrt{3}}\right\}\right], \tag{3.28}$$

with application of the inner conditions determining the constant K_0. Hence the following relation between γ_0 and a_0 is obtained:

$$a_0^3 = \frac{(\mathrm{e}-1)^3}{\gamma_0^3}\left[1 - \frac{(\mathrm{e}-1)^2}{3\gamma_0^3}\right]. \tag{3.29}$$

On the other hand, use of (3.27) in (3.25*a*, *b*) gives the spanwise velocity component $w^* = -a_0^3 u^*/(u^{*3} - a_0^3) \sim -a_0^3/\eta^{*2}$ as $\eta^* \to \infty$ from the outer constraints. Since (as before) we require as rapid a decay in w^* as possible, the constant a_0 must be zero. Thus, from (3.29),

$$\gamma_0^2 = (\mathrm{e}-1)^{\frac{4}{3}}/3^{\frac{2}{3}} \tag{3.30}$$

fixes the spanwise slip velocity $-\tilde{Q}$. This value agrees very well with that obtained numerically. In particular, the numerical results at increasing $\bar{\lambda}$-values (figure 6) indicate the behaviour

$$\hat{w}(0) \sim 0.94\bar{\lambda}^{0.674} \quad \text{as} \quad \bar{\lambda} \to \infty \tag{3.31}$$

which compares closely with the relation

$$\hat{w}(0) \sim \frac{(\mathrm{e}-1)^{\frac{4}{3}}}{3^{\frac{2}{3}}}\bar{\lambda}^{\frac{2}{3}} \quad \text{as} \quad \bar{\lambda} \to \infty \tag{3.32}$$

deduced from the analysis above.

Second, along the lower branch, the inner zone is again of thickness $O(\bar{\lambda}^{-\frac{1}{3}})$ and the appropriate expansions are

$$\hat{u} = \bar{\lambda}^{-\frac{1}{3}}\tilde{u}_1(\tilde{\eta}_1) + \bar{\lambda}^{-\frac{4}{3}}\tilde{u}_2(\tilde{\eta}_1) + \ldots, \quad \hat{v} = \bar{\lambda}^{\frac{1}{3}}\tilde{v}_1(\tilde{\eta}_1) + \bar{\lambda}^{-\frac{2}{3}}\tilde{v}_2(\tilde{\eta}_1) + \ldots, \tag{3.33a, b}$$

$$\hat{w} = \bar{\lambda}^{\frac{2}{3}}\tilde{w}_1(\tilde{\eta}_1) + \bar{\lambda}^{-\frac{1}{3}}\tilde{w}_2(\tilde{\eta}_1) + \ldots, \quad \hat{\eta} = \bar{\lambda}^{-\frac{1}{3}}\eta_1, \tag{3.33c, d}$$

so that the first terms are the same as on the lower branch, but we now have an $O(1)$ correction to $\mathrm{d}\hat{w}/\mathrm{d}\hat{\eta}$. Substitution into the vortex equations leaves $(\tilde{u}_1, \tilde{v}_1, \tilde{w}_1)$ satisfying the same equations as $(\tilde{u}, \tilde{v}, \tilde{w})$ in (3.23). The appropriate solution is effectively the same in this case, namely

$$\tilde{u}_1 = \frac{1}{\gamma_1}(\exp(1-\mathrm{e}^{-\gamma_1\tilde{\eta}_1})-1), \quad \tilde{v}_1 = \gamma_1(\mathrm{e}^{-\gamma_1\tilde{\eta}_1}-1), \quad \tilde{w}_1 = \gamma_1^2\mathrm{e}^{-\gamma_1\tilde{\eta}_1}. \quad (3.34a\text{–}c)$$

The correction terms $(\tilde{u}_2, \tilde{v}_2, \tilde{w}_2)$ satisfy the viscous balances

$$\tfrac{1}{3}\tilde{u}_1 - \tfrac{1}{3}\tilde{\eta}_1\tilde{u}_1' + \tilde{v}_2' + \tilde{w}_2 = 0, \quad \tfrac{1}{3}\tilde{u}_1^2 - \tfrac{1}{3}\tilde{\eta}_1\tilde{u}_1\tilde{u}_1' + \tilde{v}_2\tilde{u}_1' + \tilde{v}_1\tilde{u}_2' = \tilde{u}_2'', \quad (3.35a, b)$$

$$-\tfrac{2}{3}\tilde{u}_1\tilde{w}_1 - \tfrac{1}{3}\tilde{\eta}_1\tilde{u}_1\tilde{w}_1' + \tilde{v}_1\tilde{w}_2' + \tilde{v}_2\tilde{w}_1' + 2\tilde{w}_1\tilde{w}_2 = \tilde{w}_2', \quad (3.35c)$$

where $\tilde{u}_2(0) = \tilde{v}_2(0) = 0$ in order to satisfy the no-slip condition and the prime now denotes differentiation with respect to $\tilde{\eta}_1$. After some working we obtain the following differential equation for $\tilde{v}_2(\tilde{\eta}_1)$:

$$\tilde{v}_2''' - \tilde{v}_1\tilde{v}_2'' - 2\tilde{w}_1\tilde{v}_2' - \gamma_1\tilde{w}_1\tilde{v}_2 = \tfrac{4}{3}\tilde{u}_1\tilde{w}_1 - \tfrac{1}{3}\tilde{\eta}_1\gamma_1\tilde{u}_1\tilde{w}_1 - \tilde{\eta}_1\tilde{w}_1\tilde{u}_1' + \tfrac{1}{3}\tilde{v}_1\tilde{u}_1', \quad (3.36)$$

where the right-hand side is known from (3.34) and can be written as

$$(\exp(1-\mathrm{e}^{-\gamma_1\tilde{\eta}_1})-1)\,\mathrm{e}^{-\gamma_1\tilde{\eta}_1}[\tfrac{4}{3}\gamma_1 - \tfrac{1}{3}\tilde{\eta}_1\gamma_1^2] + \exp(1-\mathrm{e}^{-\gamma_1\tilde{\eta}_1} - \gamma_1\tilde{\eta}_1)[\tfrac{1}{3}\gamma_1\mathrm{e}^{-\gamma_1\tilde{\eta}_1} - \tfrac{1}{3}\gamma_1 - \tilde{\eta}_1\gamma_1^2\mathrm{e}^{-\gamma_1\tilde{\eta}_1}].$$

Therefore, in the outer reaches of this inner region, both the radial shear and the spanwise velocity corrections tend to finite limits, with

$$\tilde{v}_2 \sim \left(\frac{\mathrm{e}-1}{3\gamma_1}\right)\tilde{\eta}_1, \quad \tilde{w}_2 \to -\frac{2(\mathrm{e}-1)}{3\gamma_1} \quad \text{as} \quad \tilde{\eta}_1 \to \infty. \quad (3.37a, b)$$

This implies the following expansions in the $O(\bar{\lambda}^{\frac{1}{3}})$ outer region:

$$\hat{u} = \bar{\lambda}^{-\frac{1}{3}}u_1^*(\eta_1^*) + \bar{\lambda}^{-\frac{4}{3}}u_2^*(\eta_1^*) + \ldots, \quad \hat{v} = \bar{\lambda}^{-\frac{1}{3}}v_1^*(\eta_1^*) + \bar{\lambda}^{-\frac{4}{3}}v_2^*(\eta_1^*) + \ldots, \quad (3.38a, b)$$

$$\hat{w} = \bar{\lambda}^{-\frac{1}{3}}w_1^*(\eta_1^*) + \bar{\lambda}^{-\frac{4}{3}}w_2^*(\eta_1^*) + \ldots, \quad \hat{\eta} = \bar{\lambda}^{\frac{1}{3}}\eta_1^*, \quad (3.38c)$$

and the dominant terms then satisfy the same inviscid balances as (u^*, v^*, w^*) on the upper branch. The matching conditions in the outer region are $u_1^*(0) = (\mathrm{e}-1)/\gamma_1$, $v_1^*(0) = -\gamma_1$, $w_1^*(0) = -2(\mathrm{e}-1)/3\gamma_1$, along with the outer boundary conditions $\mathrm{d}u_1^*/\mathrm{d}\eta_1^*(\infty) = 1$, $w_1^*(\infty) = 0$. The solution for u_1^* follows as in (3.26)ff., giving

$$\eta_1^* + K_1 = u_1^* + \tfrac{1}{3}b_1\left[\ln\left|\frac{u_1^* - b_1}{(u_1^{*2} + b_1u_1^* + b_1^2)^{\frac{1}{2}}}\right| - \sqrt{3}\tan^{-1}\left\{\frac{2u_1^* + b_1}{b_1\sqrt{3}}\right\}\right], \quad (3.39)$$

where, as on the upper branch, the constant K_1 is determined by the inner constraints. Hence we find

$$\frac{\mathrm{d}u_1}{\mathrm{d}\eta_1^*}(0) = 1 - \left(\frac{b_1\gamma_1}{\mathrm{e}-1}\right)^3, \quad (3.40)$$

whereupon the governing equations yield the relation

$$b_1^3 = \frac{(\mathrm{e}-1)^3}{\gamma_1^4}\left\{\gamma_1 - \frac{(\mathrm{e}-1)^2}{3\gamma_1^2}\right\}. \quad (3.41)$$

The solution for w_1^* is the same as on the lower branch, i.e. $w_1^* = -b_1^3 u_1^*/(u_1^{*3} - b_1^3)$, and application of the matching conditions implies, after some simplification,

$$b_1^3 = 2(\mathrm{e}-1)^3/5\gamma_1^3. \tag{3.42}$$

Finally, comparison of (3.41) and (3.42) fixes the value

$$\gamma_1^2 = (\tfrac{5}{9})^{\frac{2}{3}}(\mathrm{e}-1)^{\frac{4}{3}} \tag{3.43}$$

for the spanwise slip velocity and in particular gives the dependence

$$\hat{w}(0) \sim (\tfrac{5}{9})^{\frac{2}{3}}(\mathrm{e}-1)^{\frac{4}{3}}\bar{\lambda}^{\frac{2}{3}} \quad \text{as} \quad \bar{\lambda} \to \infty. \tag{3.44}$$

This agrees well with the numerically determined behaviour on the lower branch (figure 6) as the skin friction becomes large.

4. Computational study of the full similarity problem

A numerical investigation of the system (3.2), (3.4)–(3.6) is summarized in this section. We deal with the vortex part first and write the velocities in the Fourier-series form

$$U = U_0(\eta) + \sum_{m=1}^{M} U_m(\eta)\,\mathrm{e}^{\mathrm{i}mz} + \text{c.c.}, \tag{4.1}$$

and so on, so that periodicity of 2π in z is assumed. Here M is the number of modes taken in the computation, and c.c. denotes the complex conjugate. Substitution into (3.2) leads to a set of nonlinear ordinary differential equations for the vortex velocities. Two different methods were used to solve these (see Walton 1991), the results of which agree well. The first is a shooting method allied to a fourth-order Runge–Kutta scheme. This proved a not very efficient method, and in fact at large TS amplitudes the method struggled to obtain a converged solution. That prompted the second approach, using a finite-difference representation for the vortex equations. This method has a number of advantages over the Runge–Kutta scheme: the mesh required can be considerably coarser than the step size needed for the shooting method, so that computing time is shortened as a result; also, to obtain a new value for each velocity component, each equation need only be solved once, compared to three times in the first method. Thus it would seem that the second method is more appropriate for the calculations and, indeed, the failure of the first method as the TS amplitude is increased seemed to confirm this. Next, concerning the method of solution for the TS pressure equation the functions $\mathscr{F}_\mathrm{s}$, $\mathscr{G}_\mathrm{s}$ were found to require some care. By differentiation and some manipulation, they can be shown to be governed by the nonlinear equations

$$(\xi+\tilde{\mathscr{G}})\tilde{\mathscr{G}}'' - 2\tilde{\mathscr{G}}'^2 - \tilde{\mathscr{G}}' - (\xi+\tilde{\mathscr{G}})^2\tilde{\mathscr{G}} = 0, \tag{4.2a}$$

$$\xi^2(\tilde{\mathscr{F}}-\tfrac{1}{2})\tilde{\mathscr{F}}'' - (2\tilde{\mathscr{F}}-\xi\tilde{\mathscr{F}}')^2 - \xi\tilde{\mathscr{F}}'(\xi\tilde{\mathscr{F}}'-1) + \xi^3(\tilde{\mathscr{F}}-\tfrac{1}{2})^2 + (2\tilde{\mathscr{F}}-1)\tilde{\mathscr{F}} = 0, \tag{4.2b}$$

with $$\tilde{\mathscr{F}}(\xi) = \mathscr{F}_\mathrm{s} + \tfrac{3}{2}, \quad \tilde{\mathscr{G}}(\xi) = (\mathrm{i}\alpha\lambda)^{-\frac{5}{3}}\mathscr{G}_\mathrm{s}, \quad \xi = -\mathrm{i}^{\frac{1}{3}}\Omega/(\alpha\lambda)^{\frac{2}{3}}$$

subject to the starting conditions

$$\tilde{\mathscr{G}}(0) = \frac{\mathrm{Ai}'(0)}{\mathscr{K}(0)}, \quad \frac{\mathrm{d}\tilde{\mathscr{G}}}{\mathrm{d}\xi}(0) = \frac{\mathrm{Ai}(0)\,\mathrm{Ai}'(0)}{\mathscr{K}(0)^2}; \quad \tilde{\mathscr{F}}(0) = 0, \quad \frac{\mathrm{d}\tilde{\mathscr{F}}}{\mathrm{d}\xi}(0) = -\frac{\mathrm{Ai}'(0)}{2\mathrm{Ai}(0)}. \tag{4.2c–f}$$

Here $\mathrm{Ai}(0) \approx 0.35503$, $\mathrm{Ai}'(0) \approx -0.25882$, $\mathscr{K}(0) = \frac{1}{3}$. It is then possible to determine

$\tilde{\mathscr{F}}(\xi), \tilde{\mathscr{G}}(\xi)$ from (4.2*a–f*), for all ξ, by use of a Runge–Kutta scheme, without needing to calculate explicitly the Airy function and related functions in the TS pressure equation. The rest of this part of the procedure is described in Walton (1991).

Suitable initial guesses for the skin-friction distribution $\lambda(z)$, the wavenumber α and the frequency Ω, for a given pressure amplitude $|P|$, were obtained as follows. For simplicity here the pressure–displacement law is taken to be

$$P(z) = \alpha^2 \mathscr{H}_s, \tag{4.3}$$

as a start. If we now seek a TS pressure distribution of the form $P = \cos kz$ and assume initially that the skin-friction distribution is constant, i.e. $\lambda(z) \equiv 1$, the second term in (3.6) vanishes, leaving the relation $-k^2 - \alpha^2 = \mathrm{i}^{\frac{5}{3}}\alpha^{-\frac{1}{3}}\tilde{\mathscr{G}}(\xi)$ and implying that $\mathrm{i}^{\frac{5}{3}}\tilde{\mathscr{G}}(\xi)$ must be real. This is only possible if $\xi \approx -2.298\mathrm{i}^{\frac{1}{3}}$ and $\mathrm{i}^{\frac{5}{3}}\tilde{\mathscr{G}}(\xi) \approx -1.00087$ (e.g. Reid 1965), which results in the following equation for the wavenumber α: $1.00087\alpha^{-\frac{1}{3}} = \alpha^2 + k^2$. The solution has $\alpha \approx 0.506$ for $k = 1$, and the corresponding frequency is then deduced from above to be $\Omega \approx 1.459$. For small TS amplitudes, a uniform skin friction is a good approximation, and so the numerical procedure is initiated with the values $\alpha = 0.506$, $\Omega = 1.459$, $\lambda = 1$ and $|P| \ll 1$. Once a solution is found, these new estimates can be used as the initial guesses for the solution at larger $|P|$. In this manner the effect on the solution of increasing the TS pressure amplitudes can be investigated. The results obtained can then be compared with the analysis in §3 for the flow near a symmetry line: see also the next section.

5. Numerical results, comparisons with the analysis, and further comments

Figure 7 follows the development of the vortex skin friction at the spanwise position $z = 0$ as the TS pressure amplitude $|P|$ is increased. The different curves correspond to the computations being performed with different numbers of Fourier modes. By examining the effect on the solution of increasing M it can be seen that a large number of Fourier coefficients are activated significantly. An investigation of the behaviour of the solution with M greater than 12 was beyond the capabilities of the available computing resources. A main feature of all the computations is the failure of the numerical method to provide a converged solution once the TS pressure amplitude is increased beyond a certain value, which decreases as the mode number M is increased. It is difficult to know whether to attribute this breakdown to a sudden change in the behaviour of the solution, or to accept that some parameter in the problem is now out of the range for which this particular numerical method can obtain a converged solution. In other words, is this breakdown purely a numerical artifact or is there some underlying physical reason for its occurrence here? The former may be expected because, as mentioned earlier, the shooting method originally employed to solve the vortex equations fails to provide a solution when $|P|$ reaches a certain value, but the solution given by the second method proceeds through this point smoothly with no change in the physical nature of the solution appearing to take place. On the other hand, an alternative explanation can be put forward by comparing figure 7 with the symmetry-line curve of figure 6. The ordinates of these two plots are roughly comparable as they both represent the degree of spanwise forcing present. It is possible that at the point of breakdown the curves in figure 7 are trying to turn back on themselves in a fashion similar to that exhibited in figure 6. However, no curve analogous to the lower branch of figure 6 could be found, although many attempts were made to confirm its existence; and there is in fact a different explanation, as described below.

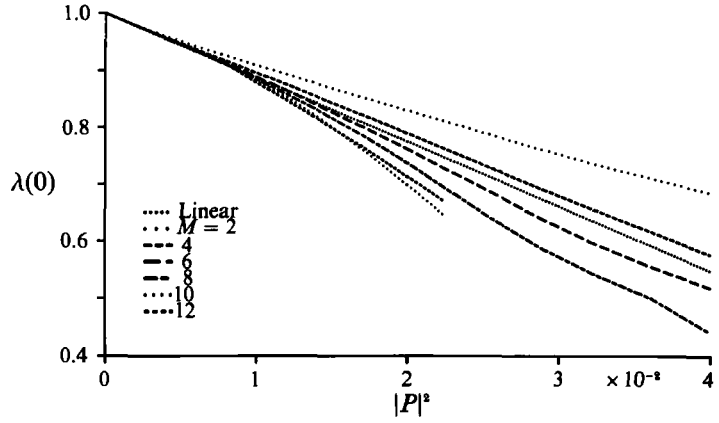

FIGURE 7. Plots of induced vortex skin friction λ at $z = 0$ versus the square of the TS pressure amplitude $|P|^2$ for different numbers of Fourier modes (M). The curve denoted 'linear' is obtained from the analysis of §3.

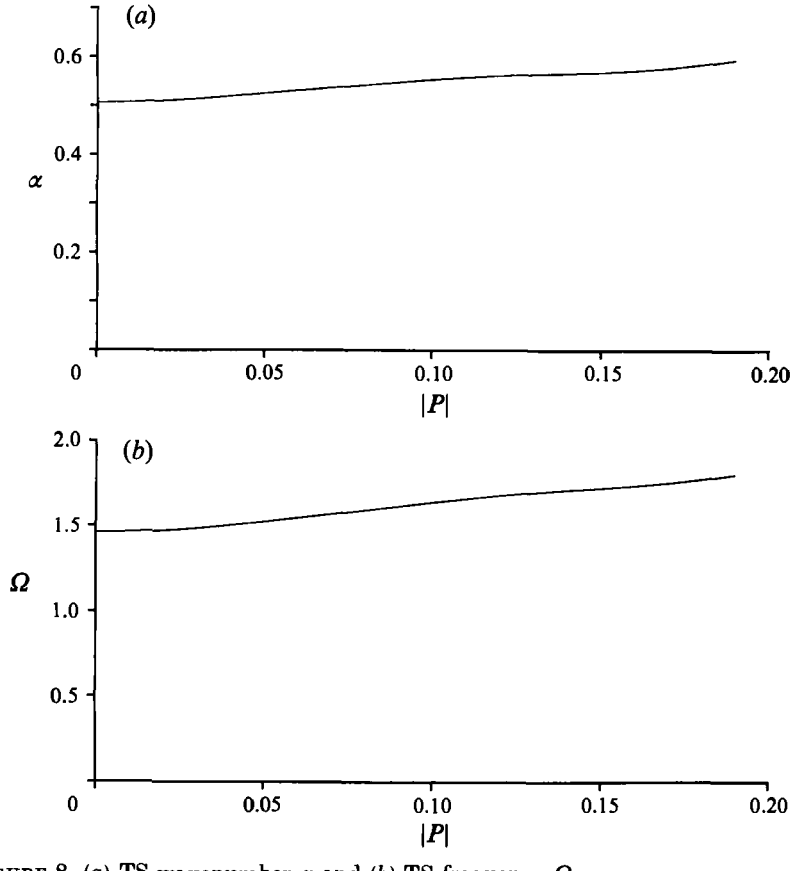

FIGURE 8. (*a*) TS wavenumber α and (*b*) TS frequency Ω, versus pressure amplitude $|P|$ with the undisturbed TS pressure given by $P = \cos z$.

The remaining figures shown are for a mode number M of 8, which appears large enough to capture most of the z-dependence without rendering the calculations too expensive to perform. Figure 8 displays the increase of TS wavenumber α and frequency Ω as $|P|$ is increased. No irregular behaviour of these parameters is

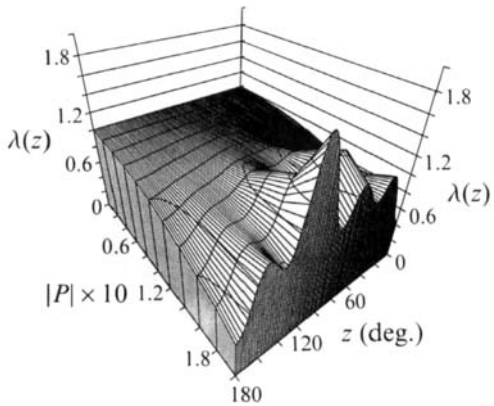

FIGURE 9. Plot of induced vortex skin friction $\lambda(z)$ versus TS pressure amplitude $|P|$ with α and Ω given in figure 8(a, b).

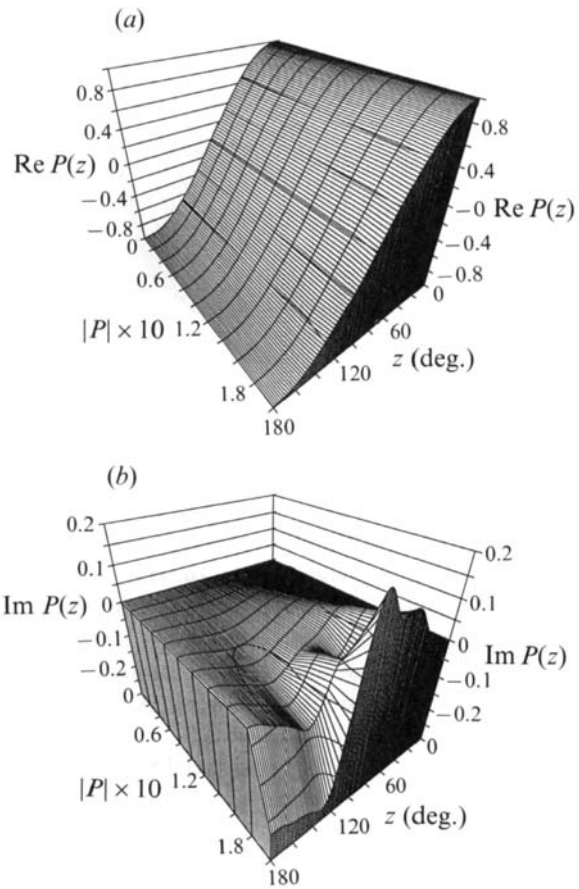

FIGURE 10. Plot of (a) the real part and (b) the imaginary part of TS pressure versus TS pressure amplitude $|P|$ with α and Ω given in figure 8(a, b).

observed as the breakdown point $|P| \approx 0.2$ is approached. Larger values of k correspond to smaller α, Ω, but these have not been investigated to any great extent as increasing k increases the number of non-zero Fourier modes, thus requiring the parameter M to be larger in the computations.

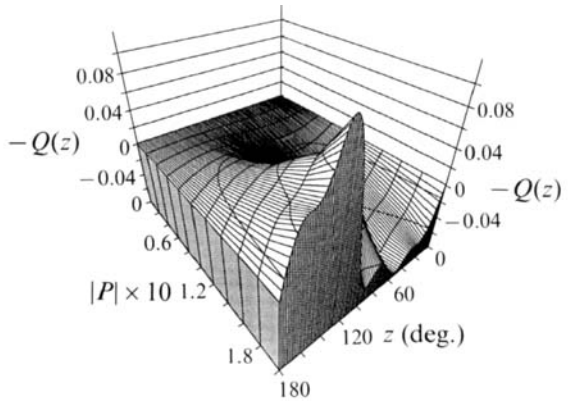

FIGURE 11. Plot of spanwise slip velocity $-Q(z)$ versus TS pressure amplitude $|P|$ with α and Ω given in figure 8(a, b).

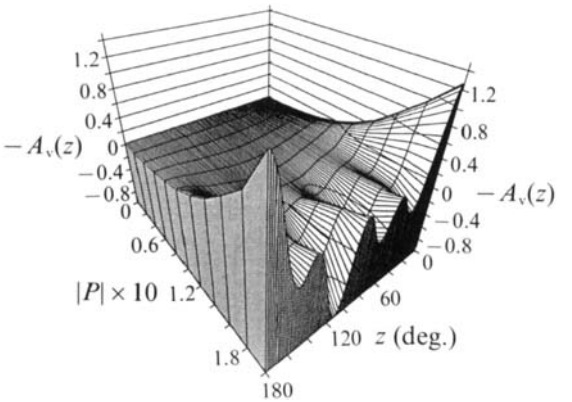

FIGURE 12. Plot of boundary-layer displacement $-A_v(z)$ versus TS pressure amplitude $|P|$ with α and Ω given in figure 8(a, b).

Figure 9 shows the behaviour of the skin-friction distribution, and this figure is essentially a three-dimensional representation of the $M = 8$ curve in figure 7. A feature of figure 9 is the relatively sudden increase in the skin friction near the position $z = 110°$; this behaviour may be related to that occurring on one of the branches of figure 6 as $\hat{Q} \to -\infty$, see also below. Again, we should emphasize the asymmetry of the breakdown, which suggests that it is not due to demanding the solution to be even about $z = 180°$.

Figure 10 shows the behaviour of the normalized TS pressure (with $P(0) = 1$) as the amplitude is increased. It can be seen from these plots that the TS pressure retains its initial cosine component, but also acquires a sine component (plotted in figure 10b) which grows rapidly in magnitude as the numerical breakdown is approached.

Figure 11 shows the response of the spanwise slip velocity $-Q(z)$ as $|P|$ is increased. The effective boundary-layer displacement $-A_v(z)$, defined by

$$U \sim \eta + A_v(z) \quad \text{as} \quad \eta \to \infty, \tag{5.1}$$

is plotted in figure 12 and indicates that there is a possibility of imminent 'separation' occurring around $z = 0°$ and 180°, where the spanwise slip velocity is small. Figure 13 presents the velocity profiles at the particular TS pressure amplitude

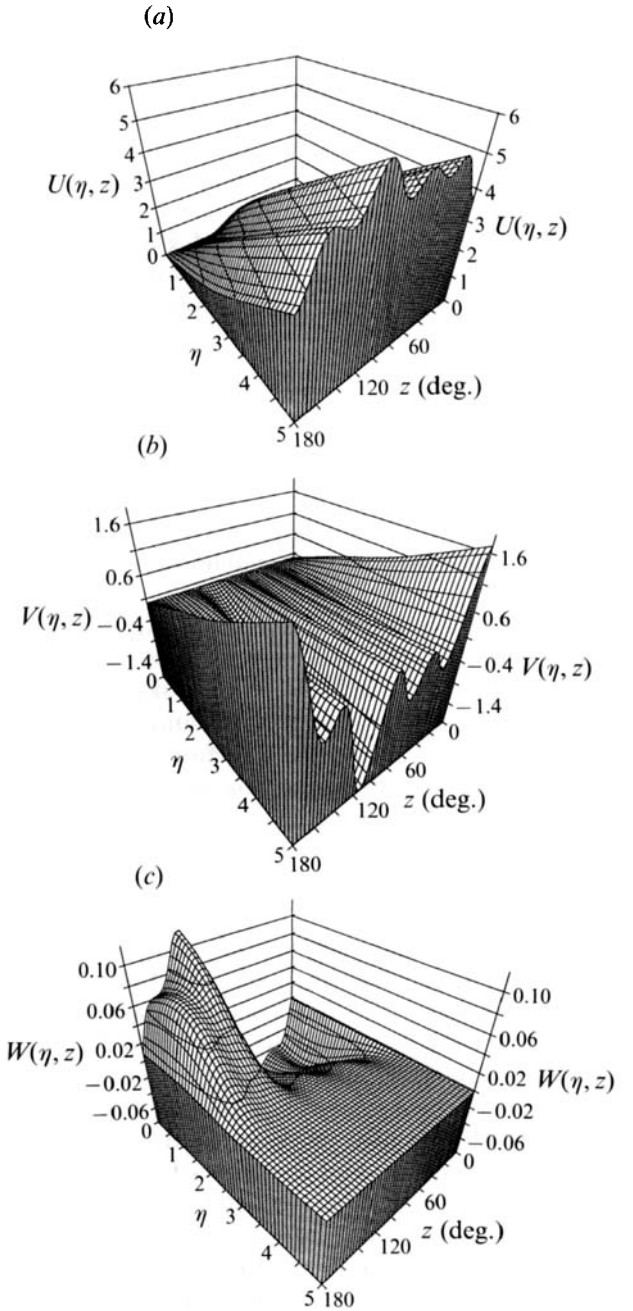

FIGURE 13. Plot of (*a*) streamwise velocity component $U(\eta, z)$, (*b*) radial velocity component $V(\eta, z)$ and (*c*) spanwise velocity component $W(\eta, z)$ at TS pressure amplitude $|P| = 0.2$ with α and Ω given in figure 8(*a*, *b*).

$|P| = 0.2$. It can be seen that near $z = 0°$, 180° the radial velocity V is large and positive, implying that fluid is being forced away from the wall, while the streamwise component U is a minimum at these spanwise locations. It is felt that the near-separated flow behaviour here can be described by an analysis very similar to that presented in §2.1.

In contrast, near the location $z = 110°$, the displacement $-A_v(z)$ reaches its maximum negative value and the skin friction $\lambda(z)$ its maximum positive value, indicating that the flow is becoming strongly 'attached' as $|P|$ is increased. In this case we may expect a local solution of the form described in §3 for the upper or lower branch to be applicable. Further evidence for this is the fact that, at $z = 110°$, both U and V are observed to attain their maximum magnitudes and the spanwise slip velocity passes through zero, while its derivative with respect to z is a maximum (see figure 11). according to the analysis of §3, and of §2.2 which also applies in the present similarity case exactly to leading order (because of the dominance of the cross-plane dependence over the streamwise dependence in both of the cases), the flow solution near the wall has the form

$$U = \frac{\bar{\lambda}^{\frac{1}{3}}}{\gamma_0}(\exp(1-e^{-\gamma_0\tilde{\eta}})-1)+O(z-z_0), \quad V = \bar{\lambda}^{\frac{2}{3}}\gamma_0(e^{-\gamma_0\tilde{\eta}}-1)+O(z-z_0), \quad (5.2a, b)$$

$$W = (z-z_0)\,\bar{\lambda}^{\frac{4}{3}}\gamma_0^2 e^{-\gamma\tilde{\eta}}+O(z-z_0)^2, \quad \eta = \bar{\lambda}^{-\frac{2}{3}}\tilde{\eta}, \quad (5.2c, d)$$

where $(z-z_0) \ll 1$, γ_0 is given in (3.30) and $\bar{\lambda}$ is the value of $\lambda(z)$ at $z = z_0 = 110°$. This behaviour agrees qualitatively with that obtained numerically and shown graphically in figure 13.

In summary here, then, solutions of the similarity form of the vortex–TS interaction have been found (§§3–5), for real values of the TS wavenumber α and frequency Ω as required, with the induced vortex skin friction and TS pressure acquiring z-dependent forms as the TS pressure amplitude $|P|$ is increased. The numerical method used (§4) breaks down at a certain value of $|P|$, and no solutions have been found beyond this point. However, the existing numerical results indicate the possibilities of attachment and separation singularities occurring in the flow solutions at certain spanwise positions, as $|P|$ is increased, these singularities being analogous with those described in §§2.1, 2.2 (and see §3) for the spatial-marching context.

Of especial interest is the separation or lift-off singularity of §2.1 for the longitudinal vortex motion. This is largely independent of the wave contribution, in local terms, granted that the wave contribution (acting as a surface slip) has already performed the important task of 'tripping' the flow from its attached two-dimensional state, upstream in the spatial setting or at earlier times in the temporal setting, or both. In the combined spatial–temporal case the next step that occurs, in faster time- and lengthscales locally, is associated with nonlinear inner–outer interaction between the displacement and the induced pressure due to the outer flow, as described by Peridier, Smith & Walker (1991*a*, *b*) in the two-dimensional version. This inner–outer pressure–displacement interaction leads in most circumstances to the finite-time breakup of Smith (1988), as Peridier *et al.*'s (1991*b*) computational studies show; see also Hoyle (1991) for the three-dimensional version. The next new step then is discussed by Hoyle *et al.* (1991, 1992), who find that significant normal pressure gradients come into operation, locally again. These can produce a further new step in which an increasingly strong azimuthal vortex is formed by winding up locally. This azimuthal vortex may represent the so-called 'first spike' of strong transition according to Hoyle *et al.* (1991, 1992), and indeed recent comparisons (by Smith & Bowles 1992) between Smith's (1988) theory and Nishioka *et al.*'s (1979) experiments show close agreement *quantitatively* concerning the occurrence of the first spike. (Recent comparisons also indicating good agreement with experiments on other related aspects of transition are given by Stewart & Smith 1992; Kachanov,

Ryzhov & Smith 1992.) So the lift-off separation singularity of §2.1 for vortex/wave interactions provides a means for small input three-dimensional disturbances to cause a cascade of scales leading to longitudinal vortex lift-off and then strong spanwise vortex formation. The repercussions of the alternative attaching-flow singularity in §2.2 remain to be considered.

In the boundary-layer application the above applies for all h in the range $1 \ll h \ll Re^{\frac{1}{8}}$, as described just below (1.1), but also for h of $O(1)$ where the vortex system gives the mean flow throughout the boundary layer.

Comments by the referees and by Dr S. N. Timoshin, and support from SERC (for A.G.W. and for computing facilities) and AFOSR (grant no. 89-0475), are gratefully acknowledged.

Appendix. On the slow-temporal case

In §2 we concentrated upon forms for the nonlinear interaction in which the only timescale present is the fast one due to the TS waves: in other words we took $\partial/\partial t$ to be identically zero in (2.1*a–c*). However, similar separation and attachment singularities are also possible ultimate forms for the case where the vortex flow operates on a slow timescale with the slow streamwise scale now absent. Once again, the analysis here is presented for the flow near a symmetry line $z = z_0$ so that the governing equations are (2.3*a–h*) with $\partial/\partial x$ identically zero, but with $\partial\bar{u}/\partial t$ and $\partial\bar{w}/\partial t$ terms added to the left-hand sides of (2.3*b*, *c*) respectively. These finite-time singularities are discussed briefly below.

A.1. *The finite-time separation singularity*

As $t \to t_s-$, we suppose the vortex components to take the form

$$\bar{u} = (t_s-t)^q F(\bar{y}) + \ldots, \quad \bar{v} = (t_s-t)^{-\gamma} G(\bar{y}) + \ldots, \quad \bar{w} = (t_s-t)^{-\gamma+N} H(\bar{y}) + \ldots, \tag{A 1a–c}$$

with $y = (t_s-t)^{-N}\bar{y}$. For a leading-order nonlinear inviscid response we require $N = \gamma - 1 > -\frac{1}{2}$. With this inequality holding, substitution of (A 1) into the modified form of (2.3) yields the balances

$$\frac{\mathrm{d}G}{\mathrm{d}\bar{y}} + H = 0, \quad -qF - N\bar{y}\frac{\mathrm{d}F}{\mathrm{d}\bar{y}} + G\frac{\mathrm{d}F}{\mathrm{d}\bar{y}} = 0, \quad H - N\bar{y}\frac{\mathrm{d}H}{\mathrm{d}\bar{y}} + G\frac{\mathrm{d}H}{\mathrm{d}\bar{y}} + H^2 = 0. \tag{A 2a–c}$$

In this case there is no restriction upon the value of q (other than it must be positive) because the streamwise velocity component F is only present in (A 2*b*), and as a linear term.

The analysis of (A 2) can now proceed in an analogous fashion to that of (2.5*a–c*) in §2.1, with the vortex shear once again found to be governed by (2.8). The corresponding expressions for G, H differ from those in (2.9) by a factor F because the streamwise velocity component is absent from (A 2*c*). The remainder of the analysis proceeds as in §2.1, except that the restriction $q > 1-2\gamma$ is not in effect here; the examples outlined there are also relevant to this case.

A.2. *The finite-time attachment singularity*

Here we suppose the flow solution to acquire the form

$$\left.\begin{aligned} &\bar{u} = F_0(Y) + \ldots, \quad \bar{v} = (t_0-t)^{-a} G_0(Y) + \ldots, \\ &\bar{w} = (t_0-t)^{-2a} H_0(Y) + \ldots, \quad y = (t_0-t)^a Y, \end{aligned}\right\} \tag{A 3a–d}$$

as $t \to t_0 -$, with $a > \frac{1}{2}$. Substitution of these expansions into the modified form of (2.3) the yields the nonlinear, cross-flow-dominated equations (2.28) once again. The solutions of these equations proceeds in an identical manner to that of §2.2.

REFERENCES

AIHARA, Y., TOMITA, Y. & ITO, A. 1985 In *Laminar–Turbulent Transition* (ed. V. V. Kozlov), p. 477. Springer.

BENNETT, J., HALL, P. & SMITH, F. T. 1991 *J. Fluid Mech.* **223**, 475.

BROWN, P. G., BROWN, S. N. & SMITH, F. T. 1992 On the starting process of strongly nonlinear vortex/Rayleigh-wave interactions. *Mathematika* (submitted).

CEBECI, T., STEWARTSON, K. & SCHIMKE, S. M. 1984 *J. Fluid Mech.* **147**, 315.

ELLIOTT, J. W., COWLEY, S. J. & SMITH, F. T. 1983 *Geophys. Astrophys. Fluid Dyn.* **25**, 77.

HALL, P. & SMITH, F. T. 1988 *Proc. R. Soc. Lond.* A **417**, 255.

HALL, P. & SMITH, F. T. 1989 *Eur. J. Mech.* B **8**, 179.

HALL, P. & SMITH, F. T. 1990 In Instability and Transition (ed. M. Y. Hussaini & R. G. Voigt). Springer.

HALL, P. & SMITH, F. T. 1991 *J. Fluid Mech.* **227**, 641.

HOLDEN, M. S. 1985 *AIAA Paper* 85-0325.

HOYLE, J. M. 1991 Extensions to the theory of finite-time breakdown of unsteady interactive boundary layers. Ph.D. thesis, University of London.

HOYLE, J. M., SMITH, F. T. & WALKER, J. D. A. 1991 *Comput. Phys. Commun.* **65**, 151.

HOYLE, J. M., SMITH, F. T. & WALKER, J. D. A. 1992 On sublayer eruption and vortex formation; part 2 (in preparation).

KACHANOV, Y. S., RYZHOV, O. S. & SMITH, F. T. 1992 Formation of solitons in transitional boundary layers: theory and experiments *J. Fluid Mech.* (submitted).

NISHIOKA, M., ASAI, N. & IIDA, S. 1979 In *Laminar–Turbulent Transition* (ed. R. Eppler & H. Fasel). Springer.

PERIDIER, V. J., SMITH, F. T. & WALKER, J. D. A. 1991*a* *J. Fluid Mech.* **232**, 99.

PERIDIER, V. J., SMITH, F. T. & WALKER, J. D. A. 1991*b* *J. Fluid Mech.* **232**, 133.

REID, W. H. 1965 In *Basic Developments in Fluid Dynamics*, Vol. 1 (ed. M. Holt), p. 249. Academic.

SIMPSON, C. J. & STEWARTSON, K. 1982*a* *Z. Angew. Math. Phys.* **33**, 370.

SIMPSON, C. J. & STEWARTSON, K. 1982*b* *Q. J. Mech. Appl. Maths* **35**, 291.

SMITH, F. T. 1979*a* *Proc. R. Soc. Lond.* A **366**, 91.

SMITH, F. T. 1979*b* *Proc. R. Soc. Lond.* A **368**, 573.

SMITH, F. T. 1988 *Mathematika* **35**, 256.

SMITH, F. T. 1989 *J. Fluid Mech.* **198**, 127.

SMITH, F. T. 1991 *AIAA Paper* 91-0331 (and *AIAA J.* to appear).

SMITH, F. T. & BLENNERHASSETT, P. 1992 *Proc. R. Soc. Lond.* A **436**, 585.

SMITH, F. T. & BOWLES, R. I. 1992 Transition theory and experimental comparisons on (*a*) amplification into streets and (*b*) a strongly nonlinear break-up criterion *Proc. Roy. Soc.* A (submitted).

SMITH, F. T. & BURGGRAF, O. R. 1985 *Proc. R. Soc. Lond.* A **399**, 25.

SMITH, F. T., DOORLY, D. J. & ROTHMAYER, A. P. 1990 *Proc. R. Soc. Lond.* A **425**, 255.

SMITH, F. T. & STEWART, P. A. 1987 *J. Fluid Mech.* **179**, 227.

SMITH, F. T. & WALTON, A. G. 1989 *Mathematika* **36**, 262.

STEWART, P. A. & SMITH, F. T. 1992 *J. Fluid Mech.* **244**, 79.

SWEARINGEN, J. D. & BLACKWELDER, R. F. 1987 *J. Fluid Mech.* **182**, 255.

SYCHEV, V. V. 1979 *Isv. Akad. Nauk. SSSR Mech. Zhid. Gaza* **6**, 21.

WALTON, A. G. 1991 Theory and computation of three-dimensional nonlinear effects in pipe flow transition. Ph.D. thesis, University of London.